SUBSALT SEISMIC ILLUMINATION STUDY

A Thesis

Presented to

the Faculty of the Department of Earth and Atmospheric Sciences

University of Houston

In Partial Fulfillment

of the Requirements for the Degree

Master of Science

By

Ana Belen Sanz Fernandez

December 2010

SUBSALT SEISMIC ILLUMINATION STUDY

Ana Belen Sanz Fernandez

APPROVED:

Dr. Christopher Liner, Chairman

Dr. John Castagna (Member)

Dr. Qingbo Liao (Member)

Repsol

Dean, College of Natural Sciences and Mathematics

ACKNOWLEDGEMENTS

This thesis would not have been possible without the help of my advisor Professor Liner. I specially thank his feedback during the study. I also want to thank to the rest of my committee members, Dr. Castagna, who guided me since the beginning of my graduate studies in the University of Houston, and Dr. Liao, without whose help and suggestions this project would never succeeded.

I would like to show my gratitude to Professors Goloshubin, Li, Hilterman, Struck, Thomsen, and Stewart for their advice during the development of this project.

I am indebted to many of my colleagues at Repsol who supported me during my research. Especially, I would like to thank Francisco Ortigosa for his help inside the company. I would like to show my gratitude to Tom Fauria for his support and for getting the permission to use the data. I want to thank Gulf of Mexico Exploration and Geophysics Groups for their collaboration during my studies. I am deeply thanked to Diego Martinez, Adrian Perarnau, Maria Donati, Pedro Munoz, and Wenying Cai for their guidance and their suggestions.

Special thanks to Ms. Birdwell and Ms. Davidson for allowing me to use TGS data for this study.

I also want to thank all my classmates and friends, especially Gabriel Gil, Maria Brito, Jianina Bastidas, Firas Jarrah, and Jonathan Parker for their help and friendship during this time.

I really appreciate the suggestions of Ivan, Jossie, Mauricio, and Cecile who edited this thesis.

I am deeply thankful to my family. My parents, my brothers Angel y Pablo, my sister-in-law Hana, and my aunt Angeles for their unconditional love and help; without them I would not be here writing this thesis. At last but not the least, I really want to thank my dear beloved Julio for his patience, understanding, support, and courage, keep on working besides the difficulties. I could not have finished any project without you.

SUBSALT ILLUMINATION STUDY

An Abstract of a Thesis

Presented to

the Faculty of the Department of Earth and Atmospheric Sciences

University of Houston

In Partial Fulfillment

of the Requirements for the Degree

Master of Science

By

Ana Belen Sanz Fernandez

December 2010

ABSTRACT

Subsalt seismic illumination is a challenge when the salt structure becomes complicated. Even using the most advanced seismic acquisition and imaging technology it is difficult to visualize subsalt targets. An illumination study can reduce exploration risk by identifying shadow areas and testing scenarios that lead to optimum image quality.

This research demonstrates that a combination of 3D ray tracing and full wavefield modeling can identify poorly illuminated subsalt areas in a case study in the Gulf of Mexico. The results show that the illumination shadow is the result of the post-critical condition at the base of salt. Ray tracing results identify the extension of the subsalt shadow areas. Also, the quality of the seismic image could improve by increasing the azimuth and offset ranges of the seismic design, extending the migration aperture, revising the velocity model, and by the use of a better migration algorithm.

This study supports the idea that a proper workflow can improve the seismic image. At times, expensive seismic algorithms cannot resolve the imaging issues; therefore, it is necessary to understand the origin of the limitation of illumination and apply the proper workflow that will enhance the quality of the seismic image.

CHAPTER INDEX

TABLE AND FIGURE INDEX

Tables

Figures

Chapter 1

INTRODUCTION

Seismic imaging is considered key to reducing uncertainty in oil exploration. The identification of the target depends on the interpretation of the seismic image. Subsalt reservoirs are trapped between the salt and the sediments. In this interface, the illumination is limited and seismic images usually have problems in target areas. An illumination study helps to understand the seismic image, improving the quality of the interpretation in the poorly illuminated areas.

Chapter 2 will review previous illumination studies. Muerdter and Ratcliff (2001) analyze the effect of salt over sediments. One conclusion is that shadow zones occur when the salt flank has a dip angle close to the critical angle. Jin and Walraven (2003) develop an illumination test based on the Sigsbee 2A model, released by the SMAART JV Consortium in 2001. The base of salt has steep dip and changes in depth, generating defocusing zones that cannot be illuminated.

Chapter 2 will continue explaining the origin of the subsalt shadows. It is shown that Snell's law and the critical angle explain the lack of illumination. The critical angle depends on the velocity contrast between salt and sediments, as well as the dip-azimuth orientation of both lithologies.

Ray theory is developed along with full wavefield modeling. Ray tracing simulates the ray paths from the horizon to the surface, helping to understand the imaging issues. Full wavefield modeling completes the analysis simulating two-way propagation, in other words the model simulates the propagation of wave from the surface to the reflection point and vice versa.

Chapter 2 also introduces the theoretical concepts that influence seismic imaging. Seismic acquisition design determines how many rays coming from the target can be registered at the surface. The survey design specifies offsets, azimuths, and shooting direction. The ideal parameters are full offset and azimuth coverage, while orientation of the seismic can vary based on the target.

The seismic image is determined by the velocity model, migration algorithm, and the aperture (Fagin, 1999). The velocity model is based on the geological model and estimates of the interval velocity gradients. The aperture depends on acquisition geometry and the target. Ideally, it should be wide enough to recover every ray coming from the target to reconstruct the correct reflector positions.

The migration algorithm is important, since it simulates how seismic waves propagate in the subsurface. The most widely used is the Kirchhoff depth migration, but it cannot handle multiarrivals and has dip limitations. Another algorithm is reverse time migration, which can simulate the full wavefield and can illuminate most dip angles.

Chapter 3 introduces the case study. The area of interest is Mississippi Canyon, located in the Gulf of Mexico. The available data includes anisotropic Kirchhoff depth migration and anisotropic reverse time migration volumes. These seismic volumes were migrated by TGS and Repsol, respectively using a vertical transverse isotropy interval velocity model developed by TGS.

This study focuses on a particular line through the 3D volume. This line is parallel to the shooting direction and exhibits seismic imaging issues: salt bodies have steep dip flanks whose surfaces are not uniform, while subsalt sediment layers cannot be interpreted easily, and seem to be located in shadow zones.

Chapter 4 exhibits the main objective of this study, which is to demonstrate that subsalt sediments are poorly illuminated for this particular dataset. This work will probe that a complete illumination study cannot only identify shadow areas, but can also explain their origin, and identify solutions to improve quality of the image.

Chapter 5 explains the proposed workflow to achieve the objective. The workflow starts by calculating the critical angle. This angle determines the shadow areas, quantifying the visualization limit for a reflection point. 3D ray tracing analysis will delineate the defocusing zones. A set of three horizons will be picked (shallow, medium and deep) in order to show illumination decreasing with depth. This study will consider three different acquisition designs: narrow, wide and full azimuth. The seismic data was acquired using the first design.

Full wavefield modeling will complete the illumination study. This model will be defined based on the available data, considering the imaging problems. The synthetic data will be migrated with two different velocity models. The first is the velocity used in the synthetic gathers generation, and the second is TGS velocity. A comparison of both migration results verifies the quality of TGS model.

Chapter 6 gives the expected results and provides some early recommendations. The critical angle changes depending on the reflector location, and as a result, its calculation will focus on one termination that exhibits a double image. Ray tracing is expected to give the highest fold values in the shallow horizon, applying the full azimuth geometry. These results are then subdivided in both near and far angles to evaluate which shooting angles from the target can reach the surface. Full wavefield modeling should demonstrate that the base of salt needs to be reviewed, and will confirm the ray tracing results.

Chapter 7 exhibits the results of the study. The critical angle explains the poor subsalt illumination. The salt flanks inclination is closer to that angle, limiting the capacity of visualization (Muerdter and Ratcliff, 2001). 3D ray tracing delineates the shadow areas. Those areas are characterized by both low amplitude and fold values. The results improve by increasing the azimuth. The accuracy of the image would improve extending the acquisition offset.

Full wavefield modeling identifies poorly illuminated areas. The results match with the ray tracing analysis. Also, this technique suggests that the modification of the velocity model would improve the seismic image. Both, the base of salt and the subsalt sediment velocity need some adjustments.

Chapter 8 completes the study, testing specified parameters. On one hand, a change in the shooting direction does not increase the illumination capacity of the subsalt reflectors in ray tracing analysis. On the other hand, an aperture extension would impact positively on the migration results of the full wavefield modeling. A shorter aperture could generate a double image of the layer terminations against the salt.

Chapter 9 proposes future research to improve seismic imaging, considering the previous results. Another illumination study should be developed to optimize the acquisition parameters, especially the offset. The exploration industry is performing analysis that quantifies the deviation of the rays by the salt-flanks in order to calculate the best acquisition parameters. Full wave propagation modeling with variable density should be included in the study in order to quantify the possible dip-azimuth ranges of illumination for each reflector. A longer migration aperture should also be tested. The data should be remigrated using a different velocity model. It is probable that the seismic image would improve using a tilted transverse isotropy instead the vertical transverse isotropy. The vertical transverse isotropy corrects the seismic image in the vertical direction, but not in the horizontal direction. Tilted transverse improves the image in both directions.

Chapter 10 finishes this study by showing the conclusions. Through a complete illumination analysis, this study demonstrates that the subsalt layers exhibit poor illumination. Snell's law explains the origin of the generation of shadow zones. If the inclination of the salt flank is closer to the critical angle, then the subsalt strata are difficult to visualize. A combination of two techniques 3D ray tracing and full wavefield modeling will delineate the shadow areas. The results of the first methodology suggest increasing both the azimuth and the offset acquisition, to improve the seismic imaging. The conclusions of the second technique propose a review of the velocity model and an extension of the migration aperture.

Chapter 2

SEISMIC IMAGING

The main objective of this study is to demonstrate the presence of subsalt shadow areas for a particular dataset. In order to achieve this goal, it is necessary to consider the previous illumination studies that have similar issues in the seismic image.

The first section of this chapter describes the methodology used by other authors to characterize and resolve the imaging issues. Ray tracing is an inexpensive technique that helps to identify variations in seismic illumination. Another technique that complements ray tracing is full wave propagation modeling, which simulates wave equation two-way propagation.

The main goal of this study also includes an explanation of the lack of illumination. Critical angle relates to the maximum reflector dip that can be illuminated and helps to explain the limitation of subsalt illumination.

The first section ends with a brief description of the algorithms used in full wave propagation modeling, such as reverse time migration.

The second section describes different acquisition designs including narrow, wide and full azimuth acquisition geometries.

The third section describes in detail the ray tracing technique, which depends on velocity model and horizon interpretation.

For reservoir characterization, it is important to understand the seismic image. As the fourth section describes, the quality of the seismic image not only depends on the acquisition design, but also the velocity model, migration aperture, and the migration algorithm.

Finally, the geological model also affects the seismic image. The dataset of this study is located in the Gulf of Mexico, and a brief description of the geological history of the area is given at the end of the chapter.

2.1. Previous illumination studies

Seismic rays experience severe bending when they reach a salt-sediment interface, where the wave speed contrast is high. Muerdter and Ratcliff (2001) studied subsalt illumination in the Gulf of Mexico and concluded key issues are:

- Decreasing maximum angle of illumination
- Fold reduction, due to the low signal-to-noise ratio
- Great reduction in amplitude (transmission losses through salt-sediment interface)
- Salt structure effect reaches the rays located less than one half of the maximum offset away from the edge of the structure
- Shape of the base of the salt further distorts the signal compared with the shape of the top; a combination of both dip angles in different directions can produce serious disruptions
- Presence of low illuminated areas when the dipping angle of the edge is close to the critical angle

The **Sigsbee2A model**, released by the SMAART JV Consortium in 2001, is a constant density acoustic velocity model and pre-stack dataset. The data do not contain free surface multiples due to a very low contrast water bottom. It illustrates the illumination issues associated with salt structures (Figure 2.1.). This model includes a rugous salt-sediment interface, whose base exhibits flat and steep dip areas. It also exhibits diffraction points, faults and subsalt structures.

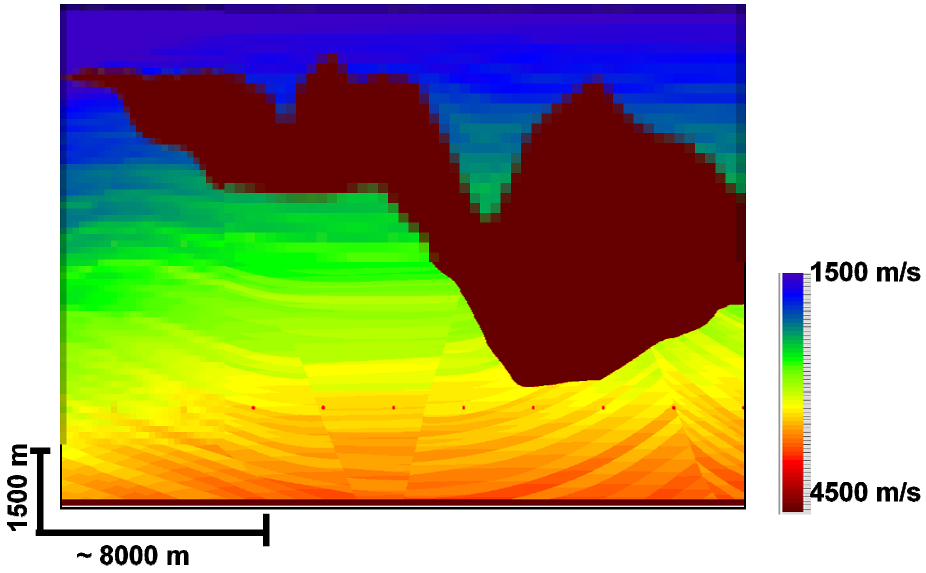

Figure 2.1. Sigsbee 2A model (released by the SMAART JV Consortium, 2001).

Ray tracing is a low-cost technique that simulates the path of the ray as it travels from the subsalt reflector to the surface (Gjøystdal et al., 2002). This methodology helps to evaluate the prospect risk by identifying issues that affect interpretation. According to Jin and Walraven (2003), ray tracing results define poor subsalt illumination zones.

Figure 2.2. shows a total illumination map which is obtained by summing energy from all directions. The black ellipses highlight the shadow areas.

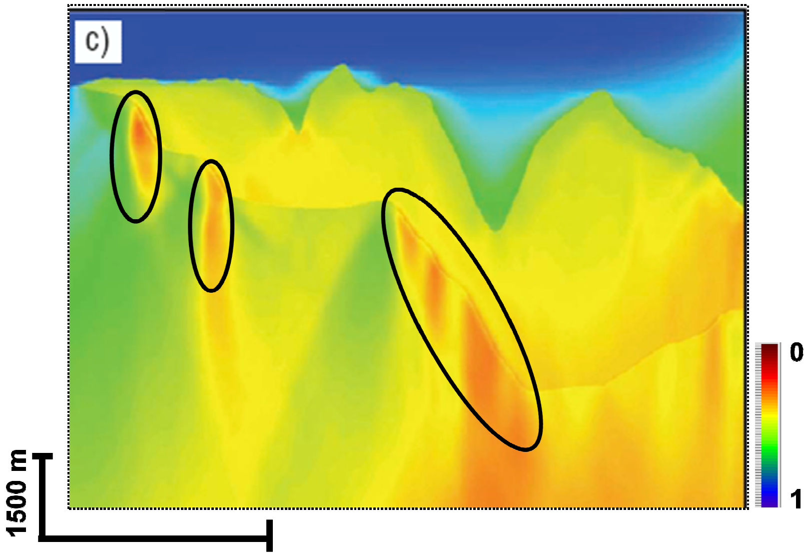

Figure 2.2. Synthetic subsalt illumination example (Modified from Jin and Walraven, 2003). The shadow zones are highlighted.

The geometrical reason for subsalt shadow areas is related to the critical angle (θ_C) computed from Snell's law. The critical angle is defined by the equation 1:

$$\sin \theta c = \frac{v_{layer}}{v_{salt}}, \tag{1}$$

where v_{layer} and v_{salt} are the interval velocities at a certain point located at the salt-sediment interface. Specifically, the maximum dip angle (θ_{max}) that can be illuminated under the salt structure is defined by the equation 2 (Liao et al, 2009):

$$\theta_{max} = \theta_c - \theta_{sed}, \tag{2}$$

where θ_{sed} represents the dip angle of the subsalt reflectors.

Ray tracing simulates the ray travelling in one direction, while wave equation modeling is a two-way computation. The results of finite difference modeling (Figure 2.3.), exhibit a good image of the top, good amplitude at the base of salt, and good collapse of diffraction points (Jin and Walraven, 2003). The shadow areas (surrounded by black ellipses), coincide with ray tracing results. Also, the amplitude is not correct in areas located under the high dipping structure (shadow areas).

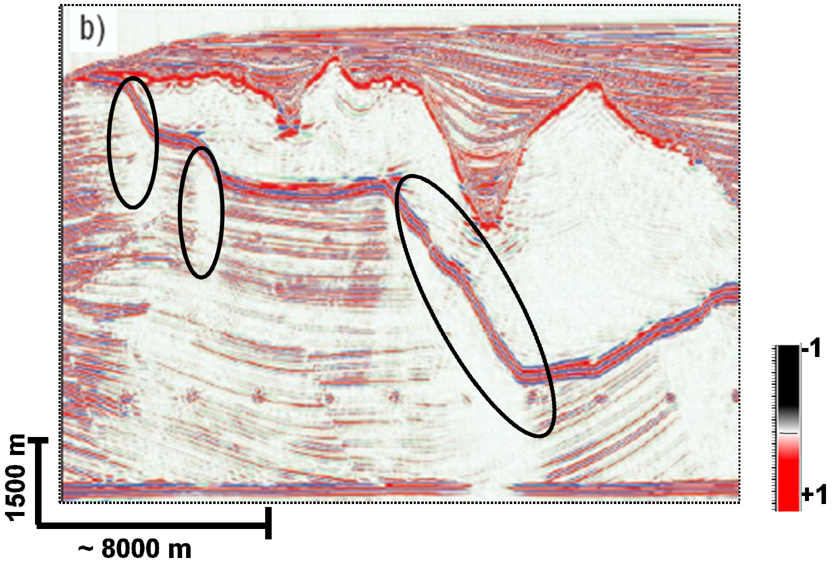

Figure 2.3. Depth image by finite difference migration algorithm (Modified from Jin and Walraven, 2003). The defocusing areas are highlighted.

The pre-stack wave equation model data can be migrated by different algorithms. For example, Jin and Walraven (2003) used wave-equation migration. The advantage of wave-equation migration is the ability to handle amplitudes, multivalued arrivals, and anti-aliasing issues in one pass (Pharez et al., 2005). In addition to the wave equation, there are other migration algorithms well-known in the industry such as reverse time migration.

Reverse time migration (Baysal et al., 1983; Whitmore, 1983) is the most advanced migration algorithm. It is a shot gather migration technique (Jacobs, 1982; Etgen, 1986), where each profile is migrated individually, followed by the summation of the imaged cubes obtained from all shots (Biondi, 2007). The algorithm can illuminate steep dipping structures. Reverse time migration is described in detail in section 2.4.4.

2.2. 3D survey design

Ray tracing results vary depending on acquisition design. Before describing the ray tracing technique, it is important to understand the different acquisition designs and how the acquisition parameters can affect the seismic image.

Anomalies in spatial sampling (associated with seismic acquisition) could cause important variations in subsurface spatial illumination. A discontinuous sampling of the data can generate amplitude anomalies and coherent artifacts, depending on the changes in density data and the complexity of the migration algorithm (Biondi, 2007).

Different shooting geometries can measure different amplitude values for the same local seismic event (Muerdter et al., 2001). In general, the best illumination is reached when the shooting direction is perpendicular to the salt-structure (Muerdter and Ratcliff, 2001). This acquisition geometry represents single-streamer marine shooting (Liner, 2004).

Narrow azimuth acquisition is a conventional design in the marine environment and only has one shooting direction. The advantage of this design is its simplicity in processing and its low computational costs. It also provides well-sampled offset data and a limited azimuth range (Biondi, 2007).

The signal is highly distorted travelling through the salt. It is necessary to use another design, such as wide azimuth, in order to record a better azimuth range. This technique includes multiple streamers following the same direction and provides more azimuth and therefore information about anisotropy in the surface and heterogeneity of the velocity field. The disadvantage of this methodology is the lower trace density of the offset plane. The sparse sampling would be an issue for pre-stack imaging since it can create some artifacts.

A full azimuth design is capable of measuring the same offset range in both inline and crossline directions. The data is acquired over 360° azimuths across the full offset range. This survey results in the maximum illumination and improves the seismic image in complex structural areas. In the Gulf of Mexico, full azimuth data can be acquired with towed systems by coil shooting with single vessel. This technique follows a pattern of overlapping circles (Moldoveanu et al, 2008). Full azimuth data can also be gathered using fixed receiver systems like OBC, OBS, or nodes (Liner, 2004).

2.3. Ray tracing

A ray is defined as a geometrical vector along the direction of wave propagation. The ray path follows Fermat's Principle: "The actual path between two points taken by a beam of light is the one which is traversed in the least time" (Liner, 2004):

$$T = \int_{p_1}^{p_2} \frac{ds}{v(x,y,z)}, \tag{3}$$

where T is the total travel time along the path from the source point p_1 to the receiver point p_2, over the short interval ds, and $v(x,y,z)$ is the velocity in that small interval.

In seismology, ray tracing is based on the concept that high frequency seismic energy follows a trajectory determined by the ray equations. Physically, these equations describe how energy travels in the same direction until it is refracted by velocity changes.

Ray tracing is computed based on the Eikonal equation (Bancroft, 2007), which is a high-frequency approximation:

$$(T^2) = \frac{1}{v^2(x_i)}, \tag{4}$$

where T is the travel time, v is the velocity and x_i the position.

Cerveny and Psencik (1983) and Sava and Fomel (2001) solve the Eikonal equation according to its characteristics, as the equation changes depending on the media. In anisotropic media, the equation is more complicated to solve. In a layer bed, as in a sedimentary basin, it is necessary to use Snell's Law at the points where the ray has contact with a structural interface.

Bancroft (2007) explains a workflow that maps the travel time on the ray paths. The density of the rays depends on both geology and grid interpolation. In salt modeling, ray tracing becomes complicated, producing multiple arrival times (amplitudes) associated with the complex structure.

2.3.1. Normal incidence ray tracing

Normal incidence ray tracing implies that the source and the receiver have the same position (Muerdter and Ratcliff, 2001). One ray represents the response of all stacked rays. This methodology is a simplification of the subsalt conditions, making it more realistic to model the entire field array.

2.3.2. 3D ray tracing

3D ray tracing analysis should be developed to understand the subsalt illumination (Muerdter et al., 2001), as it is an effective and cheap tool to understand subsalt imaging problems.

Modeling can be performed before acquisition to predict maximum illumination and calculate the best acquisition parameters (such as shooting direction), or after acquisition to identify the shadow zones and other issues that can affect interpretation and risk analysis.

Accurate amplitude modeling results will be reached by reproducing the shooting geometry that was used in seismic acquisition (Muerdter et al., 2001).

2.4. Depth imaging

Seismic migration reconstructs the image by moving events to their earth-coordinate positions. The accuracy of the final product depends on the imaging algorithm, migration aperture, velocity model and sampling of the signal (Fagin, 1999).

The imaging algorithm is the most important factor and will be discussed in detail in the next section.

Migration aperture is defined as the offset range of data included in the migration of each point. The best estimated value is double the horizontal distance of the migration of the reflector having steepest dips. The disadvantages of using large aperture values are the resulting increase in migration computing time and to include more multiples.

The migration velocity model should flatten the depth of events on seismic image gathers. There are several techniques used to update the velocity model, based on event residual curvature in image gathers.

The signal should be registered and correctly sampled. Irregularities in spatial sampling can cause important changes in the spatial illumination of the studied area. Depending on the density of the sample distribution and the algorithm, the image can be seriously affected by aliasing or artifacts (Biondi, 2007).

After migration, the depth image should represent geological reality.

2.4.1. Model building

The velocity model is one of the most important factors that control image results. Seismic velocity can change with depth, lithology, age, and pressure (Fagin, 1999).

The velocity changes do not always correspond to geological variations. Sometimes, the geological units do not exhibit a contrast in acoustic impedance. In those cases, it is better to use a frame which does not depend on structural interpretation.

In the Gulf of Mexico, the sediment velocity above the salt does not depend on geological structure. In contrast, subsalt velocity variations mostly respond to structure making it possible to build a hybrid velocity model.

Model-based velocity analysis is a technique which uses a structural framework. The workflow takes time gathers as input and obtains a final 3D cube velocity in depth. According to Fagin (1999), the workflow has two phases. The first part is generated based on a sequential layer stripping, with each layer analyzed successively. The second part is iterative and applies successive depth migration to find the correct position of all the layers. The quality of the initial model will determine the number of iterations needed to generate an accurate final model. After applying the final migration velocity model, events should be flat in image gathers.

The velocity model can be refined using the results of depth imaging using coherency or tomography (Fagin, 1999).

2.4.2. Migration algorithm

There are many migration algorithms which try to find the correct position of the recorded data in the subsurface. This study, however, will focus on two widely used migration algorithms: the Kirchhoff pre-stack depth migration and reverse time migration.

2.4.3. Kirchhoff depth migration

This method is one of the most commonly used by industry. The Kirchhoff integral used for migration (Schneider, 1978, Docherty, 1991, Audebert, et al., 1997, Bleistein and Gray, 2001) is based on Green's theorem (Morse and Feshbach, 1953) and represents an integral solution of the wave equation. According to Biondi (2004), the approximation integral is:

$$I(r) \approx \sum_{i} W_i(r,m,h)D\big[t_D(r,m,h),m_{i,}h_i\big], \tag{5}$$

where the image $I(r)$, defined in three-dimensional space $r(x,y,z)$, is equal to the data values (D), evaluated in the diffraction time t_D and weighted by a factor $W.$ W_i stands for the correct amplitude values, $m_{i,}$ is the midpoint location, and h_i indicates the offset positions.

The technique is based on diffraction summation (Bezahd and Pajchel, 2006). Physically, it means that the diffraction from an isolated point in the subsurface will be equivalent to an event with the same shape as the summation surfaces.

Diffraction time is not easy to compute in salt basins. There are different techniques to calculate t_D, all of them based on the Eikonal equation (high frequency approximation of the wave equation).

The accuracy of the Kirchhoff depth migration depends on the methodology chosen to calculate the summation surfaces (Biondi, 2007). The most efficient method is the direct solution of the Eikonal equation by the finite difference method (Van Trier and Symes, 1991). The finite difference method has the disadvantage that it can only compute one arrival, generally the first. In some cases, the first arrival does not carry the most important part of the wavefield energy and should not be considered in the migrated image.

Ray tracing is more time consuming than finite difference modeling, but it allows the selection of the arrivals used in migration.

The image $I(r)$ is resolved iteratively at each point, and is the result of the summation of the contribution of every input trace within the migration aperture. The Kirchhoff migration algorithm calculates the diffraction surface based on the ray path between source and receiver. Each offset plane is migrated independently and then summed together to generate the stacked image. The full process is divided in two phases: summing input data points with the same offset, and then summing along the offset (Bezahd and Pajchel, 2006).

Jones and Fruehn (2003) enumerate the factors that affect the frequency in Kirchhoff pre-stack depth migration. Assuming the velocity model is correct, the most important factors that can affect the image quality are: adequate sampling of the velocity field, adequate sampling of the input data on the acquisition subsurface, and adequate sampling within the Fresnel zone at the image point. To avoid shallow artifacts, the authors propose the use of non-linear interpolation or the use of a smaller grid.

The history of 3D Kirchhoff depth migration

3D Kirchhoff pre-stack depth migration has been performed since 1995 (Jones et al., 2008). In that year, the technique consisted in of full offset 3D pre-stack depth migration with an isotropic single arrival, a dip limit of 90°, and later a turning ray. Ratcliff et al. (1995) applies this technology to image a subsalt play in the Gulf of Mexico.

In 2000, Kirchhoff depth migration was improved by generating seismic gathers as an output. Billette et al. (2000) apply this technique in the Gulf of Mexico and Trinidad.

In 2002, anisotropy was incorporated to the Kirchhoff depth migration as a single arrival. Meek et al. (2002) proposed a method of 3D anisotropic model building, tested in the Belida Field in Indonesia. Sarkar and Tsvankin (2003) analyzed the P-wave image gathers in transversely isotropic media with a vertical symmetry axis (VTI).

Characteristics of the Kirchhoff pre-stack depth migration

Kirchhoff depth migration is an integral method and is usually implemented in the depth domain, but can also be applied in the frequency domain (Jones et al, 2008).

The separation of imaging from the travel times calculation, allows subset volume computation without the need for full volume imaging. For this reason, the Kirchhoff algorithm is efficient with respect to computing time.

Advantages

The Kirchhoff depth migration algorithm delivers a subset of the imaged volume, including offsets or angles, and it is reportedly cost-effective for iterative model building.

Disadvantages

Kirchhoff only integrates energy that has traveled along one path. Unfortunately, it considers the first arrival, which may not represent the largest part of the energy of the wavefield.

The velocity field is coarsely sampled for travel time computation and the arrival times are interpolated back to seismic spacing, which can misrepresent high lateral velocity variations (such as the top of the salt body).

2.4.4. Reverse time migration

Reverse time migration (Baysal et al., 1983; Whitmore, 1983) is a wave equation migration continuation method and requires high computational cost. It is based on the shot gather migration technique (Jacobs, 1982; Etgen, 1986), where each profile is migrated individually followed by the summation of the image cube obtained for each shot (Biondi, 2007).

This technique computes two wavefields independently: the source to the subsurface reflection point and the reflection point to the receiver at the surface.

The source wavefield is propagated time forward, while the recorded wavefield is propagated backward in time, leading to the name reverse time migration. The final image is the cross-correlation of the two wavefields evaluated at zero time (Claerbout, 1971).

The wave equation is linear with respect to the source, so shot profile migration can be generalized to image collections of gathers.

According to Biondi (2008), the image is computed applying the following condition:

$$I\left(z_{\xi}, x_{\xi}, y_{\xi}\right) = \sum_{s} \sum_{g} P^{g}\ (t, z = z_{\xi}, x = x_{\xi}, y = y_{\xi}; s_{i}) P^{S}\ (t, z = z_{\xi}, x = x_{\xi}, y = y_{\xi}; s_{i}). \qquad (6)$$

where: $I\left(z_{\xi}, x_{\xi}, y_{\xi}\right)$ is the image; $P^{S}\ (t, z = z_{\xi}, x = x_{\xi}, y = y_{\xi}; s_{i})$ and $P^{g}\ (t\ z = z_{\xi}, x = x_{\xi}, y = y_{\xi}; s_{i})$ are respectively the source wavefield and the recorded wavefield for the i_{th} source function s_{i} as functions of time and subsurface location (z, x, y).

The previous equation differentiates between image space $\left(z_{\xi}, x_{\xi}, y_{\xi}\right)$ and real space location (z, x, y). In practice, both spaces are usually equivalent.

History

According to Boarding and Lines (1997), Hemon was the first author who mentioned reverse time migration in 1978 and used the finite difference method for the wave equation. Whitmore, at a migration workshop during the 1982 SEG Annual Meeting, showed the successful application of the method for imaging overthrust folds and overhanging salt domes.

In 1983, three papers (McMechan, Baysal et al. and Whitmore) treated the subject under different names. Baysal was the first author using term reverse time migration, and used the Fourier method. Nowadays in the oil industry, the most popular method used to solve the wave equation for reverse time migration is the finite difference method. In simple words, this technique allows the wavefield to propagate backward to the original depth point where the reflections were generated (Boarding and Lines, 1997).

McMechan and his students at the University of Texas in Dallas made advances in the technique, extending reverse time migration: from post-stack to pre-stack, from isotropic to anisotropic (Dong and McMechan, 1993), and from acoustic to elastic.

As hardware computational capability improved, the use of this technique became more popular. Since 2006, reverse time migration has been extended to VTI and TTI by many researchers thanks to a pseudo-acoustic approximation (Zhou et al, 2006; Du et al, 2008; Duveneck, 2008; Fletcher et al, 2008). Solutions to instabilities appearing for TTI equation have been proposed by Zhang and Zhang (2009) and Fletcher et al (2009).

Characteristics

Time reversed seismic wave propagation requires time-dependent surface boundary conditions, which allow the wavefield to be backward time propagated at half of the medium's velocity (Boarding and Lines, 1997).

Each depth slide of the wavefield is calculated from the previous, so it is necessary to compute the full image volume.

Advantages

Reverse time migration provides a general solution of the wave equation, which can be extended to two-way time. Computationally, waves can be propagated forwards or backwards in time with the same level of complexity.

This algorithm illuminates without angle limitation and is very useful in complex geological environments (overthrust fold or high dip salt domes).

The amplitude treatment is automatic.

Disadvantages

Reverse time migration exhibits certain negative features. To begin with, it is an expensive algorithm compared with other imaging methods. It is necessary to compute the whole volume, so subset areas of interest cannot be migrated separately.

It is necessary to make restrictive assumptions in order to perform iterative model building.

Futhermore, reverse time migration can exhibit artificial reflections coming from the boundaries of the domain (Clapp and Fu, 2010). There are different techniques to resolve this problem, including introduction of a damping region around the computation domain (Cerjan et al., 1985), introduction of a boundary condition that attempts to kill energy propagating at some limited range of angles perpendicular to the boundary (Clayton and Engquist, 1980), or application of a perfectly matched limit (PML) (Berenger, 1996), which simulates propagating a complex wave whose energy decreases as it approaches the boundary (most effective and expensive).

Yan and Xie (2009) affirmed that reverse time migration produces low wavenumber artifacts that mask the geological structure. This issue becomes critical in areas with high velocity contrast like salt structures.

2.5. Anisotropy

Seismic anisotropy is defined as “the dependence of seismic velocity upon the angle” (Thomsen, 2002). Subsalt seismic events can be affected by this phenomenon. Migration and modeling should include the anisotropy effect to ensure accuracy in event positioning (Jones et al., 2008). In areas with strong lateral variation, it is necessary to include anisotropy in the migration, to avoid depth estimation errors which can increase drilling costs or lead to a dry hole.

It is difficult to calculate anisotropic parameters in exploration areas because of sparse well data. Geological formations exhibit anisotropic behavior due to different physical reasons (Tsvankin, 2001; Thomsen, 2002). The presence of anisotropy (VTI type) in sedimentary rocks is a consequence thin layering and intrinsic anisotropy due to shale.

General anisotropy depends on 21 elastic coefficients. The estimation of those parameters is beyond the computational capability of the industry. Therefore, geophysicists usually simplify to symmetry classes (VTI, HTI, TTI) that have two anisotropy parameters ε and δ (Thomsen, 1986):

$$v_H^2 = v_V^2 \, (1 + 2\varepsilon), \tag{7}$$

$$v_N^2 = v_V^2 \, (1 + 2\delta), \tag{8}$$

where v_H is the horizontal velocity, v_V is the vertical velocity, and v_N is the NMO velocity.

The estimation of TTI parameters is more difficult than VTI parameters. Usually, the calculations are based on the interpretation of dipping strata that are characterized by VTI.

2.6. Geological history of Gulf of Mexico

The continental margin which underlies the Gulf of Mexico originated during late Triassic and early Jurassic time with the breakup of Pangea when Africa/South America separated from North America. Rift phase deposits were Triassic to lower Jurassic lacustrine and red bed clastics, followed by massive evaporites and carbonates deposited during a drift phase in latest Jurassic time. During Cretaceous time, a stable carbonate platform developed with carbonate banks accumulating around the edges of the basin.

A general uplift of the North American continent during late Cretaceous and early Tertiary time provided vast amounts of clastic sediment that were transported into the northwestern Gulf of Mexico. As the basin subsided, these large volumes of sediment were deposited as successively younger wedges of off-lapping strata. The supply of sediment, being out of phase with the load-induced subsidence, created multiple transgressive and regressive depositional environments. A large volume of clastics was supplied to the basin, related to mountain building during the Tertiary and later during the Quaternary due to continental glaciation. As a result, basin subsidence was overwhelmed and the Gulf of Mexico margin prograded seaward (Baud et al., 2000).

The salt precipitated in the late Jurassic was loaded and deformed by the subsequent deposition of the post-Jurassic clastics. Until relatively recently, almost all

Gulf of Mexico salt structures were thought to be piercement-type structures connected to original salt deposits. It has since been demonstrated that much of the salt is allochthonous, and no longer connected to the underlying autochthonous Jurassic salt. The Cenozoic structural evolution of the northern Gulf of Mexico Basin is largely controlled by the progradation of clastic wedges, the withdrawal of salt from the autochthonous level, and subsequent deformation at the allochthonous level. During progradation, progressive salt withdrawal from tabular salt bodies on the slope formed salt-bounded minibasins. Salt-withdrawal minibasins with flanking salt bodies occur as both isolated structural systems and components of salt-based detachment systems.

Chapter 3

CASE STUDY

The area of interest is located in the Gulf of Mexico's Mississippi Canyon, which exhibits alochtonous salt bodies. The sediments have been deposited since the Late Jurassic. The strata are composed of interbedded siliciclastic sandstones and shales. Salt displacements generated extensive normal faults, crossing the sediment layers.

The available dataset is composed of two migrated stack depth volumes, located in the same exploration area in the Gulf of Mexico. Both volumes correspond to the same narrow acquisition survey (Appendix 1), and are the result of the same pre-processing and the same shot-gathers generation. They have also been migrated by the same v_p velocity field (Figure 3.1.), which is anisotropic (vertical transverse isotropic). The main difference is the migration algorithm: pre-stack anisotropic Kirchhoff depth migration (Figure 3.2.) and anisotropic reverse time migration (Figure 3.3.). The migration apertures are different: 10 km and 12 km, respectively. The seismic processing sequence appears in Appendix 2.

The studied area covers a small part of the total survey and does not have any well data in its proximity. Also, there is no seismic migrated gather available for this study. The dimensions of the seismic section displayed in Figures 3.1. and 3.2. are 31 km x 12.5 km.

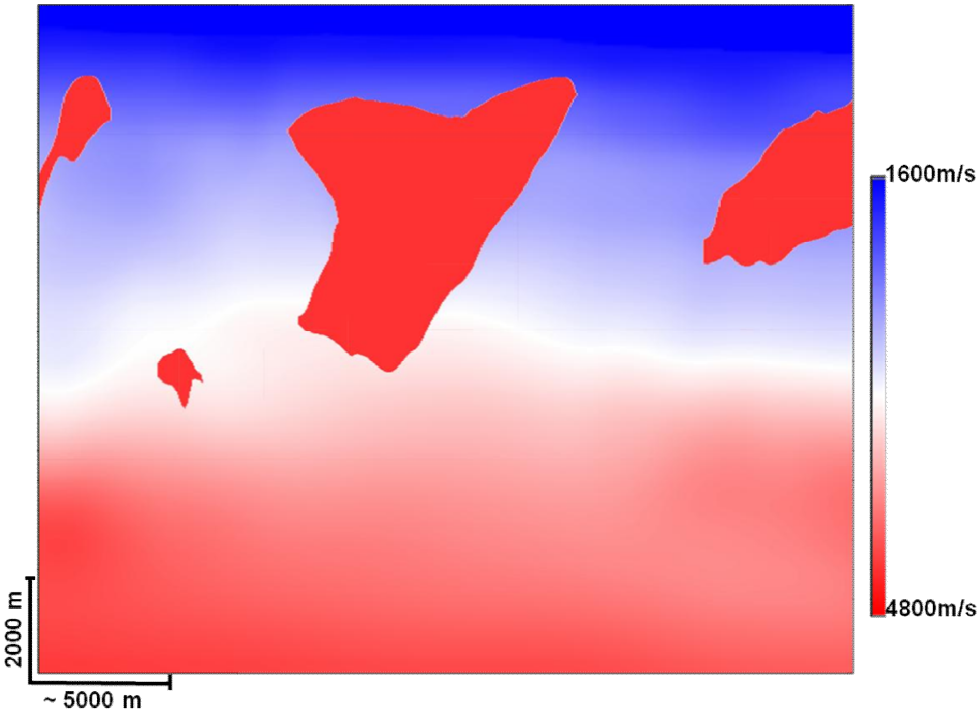

Figure 3.1. 2D slice of the 3D anisotropic v_p velocity field.

Figures 3.2. and 3.3. show the seismic image volumes for anisotropic Kirchhoff depth migration and anisotropic reverse time migration (respectively). In general, the tops and bases of the salt bodies are well defined in both images. anisotropic Kirchhoff depth migration has higher frequency and exhibits a better resolution of the sediments in the areas not affected by the influence of the salt bodies. As expected, anisotropic reverse time migration improves the continuity of the subsalt sediment layers.

Besides the differences, both images exhibit some shallower stratification with an increasing sediment wedge associated with the structure (upper right in Figures 3.2. and 3.3.). The terminations of the layers are folded and change in depth. On the other hand, Kirchhoff cannot illuminate the terminations against the salt, showing a noisy image.

Anisotropic reverse time migration exhibits a double image of the terminations in the shadow zones, following two different trends. The first trend is flat and follows the compaction. The second shows steep pseudo-parallel dip planes, opposite to the stratification different than the fault planes.

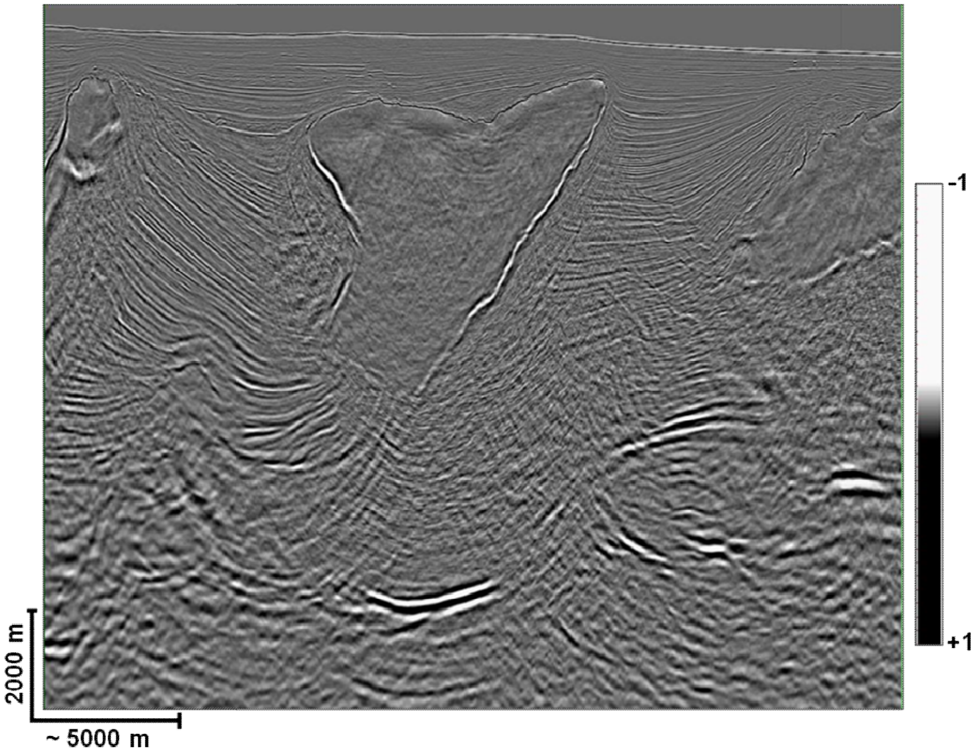

Figure 3.2. 3D anisotropic Kirchhoff pre-stack depth migration. 2D section is shown coincident with velocity model in Figure 3.1..

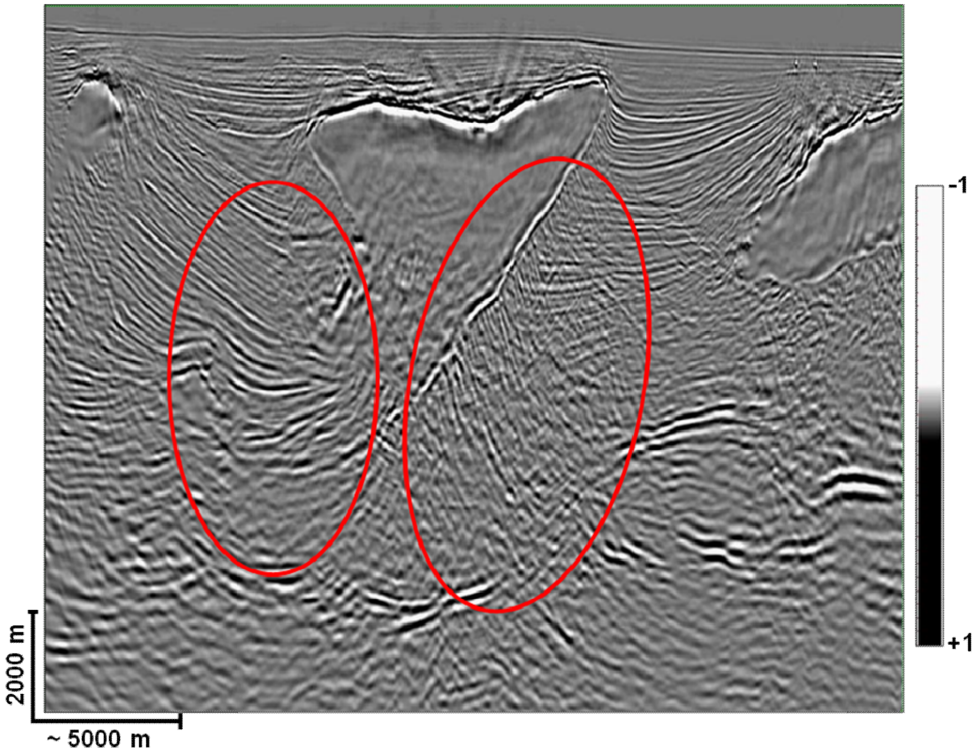

Figure 3.3. 3D anisotropic reverse time migration shown along same line as Figure 3.2. Areas of this illumination study are highlighted.

Chapter 4

OBJECTIVES

This study will demonstrate with a complete illumination analysis, that the subsalt sediments (see Figures 3.2. and 3.3.) are poorly illuminated in the area of interest. This main objective can be subdivided in three parts:

- Find the origin of the shadow areas. This point is central to understanding the reason behind the illumination issues.
- Highlight the extension of the shadow zones. The boundary definition is important for interpreters, in order to evaluate the risk of prospects based on quality of the seismic image. Also, this study will evaluate if the limits of the shadows depend on seismic acquisition details. This analysis will test three different acquisition designs: narrow, wide, and full azimuth.
- Propose solutions to improve the accuracy of the image. The success of an exploration prospect depends on image quality, especially in the absence of well data. Related with the previous objective, there are some techniques that could partially resolve the illumination issues. A change in acquisition parameters (offset, azimuth, and shooting direction) can impact the seismic image. The migration aperture is another parameter that can generate different results. Finally, the wrong velocity model can introduce noise in the image, or even worse it can generate false structures.

Chapter 5

METHODOLOGY

A complete illumination study helps to understand subsalt imaging problems, as exhibited in Jin and Walraven (2003) with Seigsbee2A Model (Smaart JV Consortium, 2001). The first step of the workflow is to find the origin of the poorly illuminated areas. As noted earlier, the shadow areas are generated by the high velocity contrast in the salt-sediment interface and by the relative orientation of salt face and sediment layering. The critical angle and salt face orientation determine the maximum angle that can be captured at the acquisition surface for a certain subsalt reflector.

The second part of the workflow defines the boundaries of the subsalt shadow areas using 3D ray tracing. In Figure 3.3., the areas of interest are circled in red.

In order to complete the illumination study, it is necessary to simulate two-way ray paths with full wavefield modeling. The results help to understand the illumination issues and confirm the ray tracing results.

The combination of ray tracing and full wavefield modeling will define the extension of the shadow areas, and analysis of the results suggest solutions to improve seismic image quality.

5.1. Critical angle estimation

The critical angle can be calculated using Snell's Law (equation 9):

$$\sin\theta c = \frac{v_{layer}}{v_{salt}}, \tag{9}$$

where v_{layer} and v_{salt} are the interval P-wave velocities at a reflection point situated at the interface between sediments and the salt body.

The maximum subsalt sedimentary dip angle (θ_{max}) that can be imaged is (Liao et al, 2009):

$$\theta_{max} = \theta_c - \theta_{sed}. \tag{10}$$

In our case study, the angles greater than θ_{max} represent the dip angles coming from a sediment layer that cannot be registered at the surface due to the steep dip of the base of salt. The results section will explain this point in detail.

5.2. Ray tracing

A set of three horizons were picked at levels of increasing depth. I term these shallow, medium, and deep. In Figure 5.1. , those events are shown in blue, red, and yellow respectively.

The horizons are chosen based on two main criteria. The horizons follow seismic events exhibit in the anisotropic reverse time migration and anisotropic Kirchhoff depth migration volumes. The sediment terminations against the salt bodies are mostly flat.

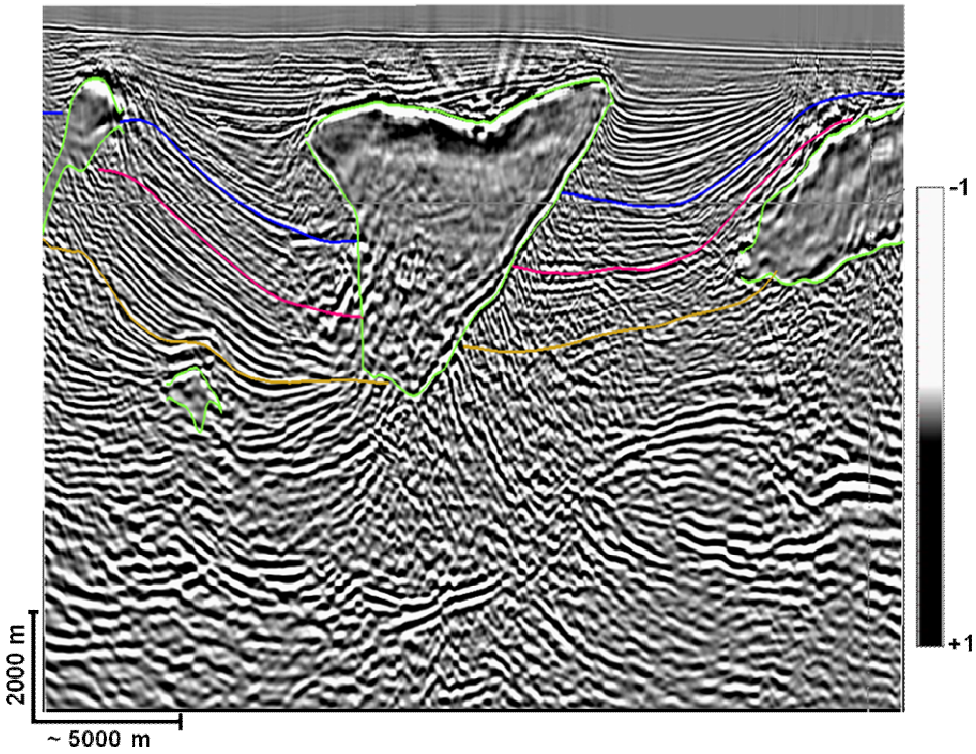

Figure 5.1: Anisotropic reverse time migration showing salt (green), shallow (blue), medium (red), and deep (yellow) horizons.

3D ray tracing is calculated using the Epos 3 software from Paradigm simulating one-way travel from each horizon to the surface. The input data are the TGS isotropic velocity model and the shallow, medium, and deep grids.

The ray tracing workflow is as follows:

1. Full azimuth acquisition is simulated an ideal case where it is possible to recover every ray that travels from the target and hits the surface inside the acquisition grid (at sea level). The vertical projection of the reflection point is located at the center of the acquisition grid. Figure 5.2. represents a scheme of this

acquisition geometry. The parameters included in the computation are enumerated in Table 5.1..

2. Narrow azimuth acquisition is simulated by filtering the full azimuth results. The illumination parameters are based on a narrow azimuth survey acquired in the studied area (Appendix 1). Table 5.1. shows the narrow azimuth ray tracing parameters. Accurate amplitude modeling results will be reached by reproducing the shooting geometry that was used in the seismic acquisition (Muerdter et al., 2001).

3. Wide azimuth acquisition is simulating by filtering the full azimuth ray tracing results. In this case, the crossline offset range is 100 – 4200m. The rest of the parameters are the same as the narrow azimuth acquisition. These parameters are based on a seismic design that is planned to shoot in the area of interest. Table 5.1. shows the wide azimuth parameters. Wide azimuth design could be a possible solution to both reduce the shadow areas and to improve the quality of the seismic image. Figure 5.2. represents a scheme of this acquisition design.

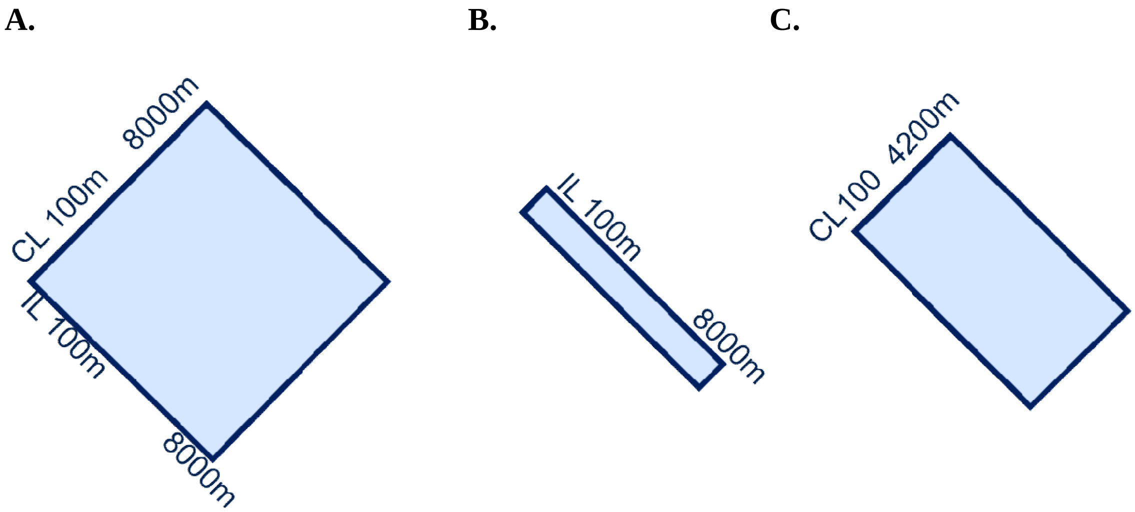

Figure 5.2. Comparison between the three different acquisition geometries applied in ray tracing computation. A. Full azimuth. B. Narrow azimuth. C. Wide azimuth.

		Full azimuth	**Narrow azimuth**	**Wide azimuth**
Inline offset range		100 - 8000 m		
Crossline offset range		100 - 8000 m	100 - 1000 m	100 - 4200 m
Shooting parameters	Direction	45° NW-SE		
	Dip range	0 – 30° (step: 1°)		
	Azimuth range	-45° – 135° (step: 5°)		

Table 5.1. Ray tracing parameters.

After ray tracing, the three different horizons with the three acquisition designs will be compared with the seismic images. In order to have a better understanding of the results, ray paths from different reflectors will be displayed.

Comparison of the results for each case will help suggest some acquisition parameters that can capture more rays coming from the subsurface.

5.3. Full wavefield modeling

Ray tracing simulates one-way traveling from the reflector to the surface, while full wavefield modeling simulates the two-way path travelling from the surface to the reflector and from the reflector to the surface. Full wavefield modeling is accomplished using 2D acoustic finite difference modeling, and includes diffraction, multipathing, and other finite frequency phenomena.

In order to be comparable with ray tracing study, this model is isotropic with constant density. The main difference between the design of ray tracing and full wavefield modeling is the dimensionality. Full wavefield modeling is 2D in the line of interest while the ray tracing is computed in 3D.

The workflow used to generate full wavefield modeling starts with the interval velocity model building, which is based on TGS velocity model and is called the revised velocity model in this study. The original TGS velocity model is referred as original.

The following step of the workflow is the model parameterization. This section explains the numerical implementation and the application conditions done to build the model. Then, a wavefield snapshot analysis is performed. The results of this analysis show how the wavefront propagates in the model. The following step is shot gather generation. If the output is correct, then all shot gathers are generated. The synthetic gathers are computed with the revised velocity. The gathers are then sorted by shot location, offsets are subsampled by a factor of 2, and the direct arrival is muted. The shot gathers are then migrated using the revised and original interval velocity volumes, using reverse time migration. The code generates two different outputs: the post-stack migrated image and a Hessian illumination matrix. Both results are filtered to eliminate high frequency.

5.3.1. Velocity model building

The full wavefield modeling should agree with the ray tracing results, because shadow areas are generated by a combination of velocity contrast between the salt and the sediments and the relation of the dip angles between them.

The velocity model includes twenty two horizons. Horizon picking is done in 2D, except the shallow, medium, and deep horizon used in ray tracing analysis. The interpretation follows the studied line of anisotropic Kirchhoff depth migration (Figure 5.3.). The interpretation assumes that the terminations against the salt are mostly flat.

The salt shapes are not correct in the TGS velocity model at certain points, especially in the Y-shaped salt body. Therefore, some tops and bases have been slightly modified. If the salt body grows moving the salt-sediments interface deeper, then the interval velocity changes from sediment to salt values. The velocity increase pushes down the seismic events.

The sediment velocity trend does not match with a high amplitude layer at the low part of the section. This event is probably a hard layer that could be either a second salt body, or a carbonate. In either, the velocity should be higher than the original sediment velocity and it was assigned salt velocity.

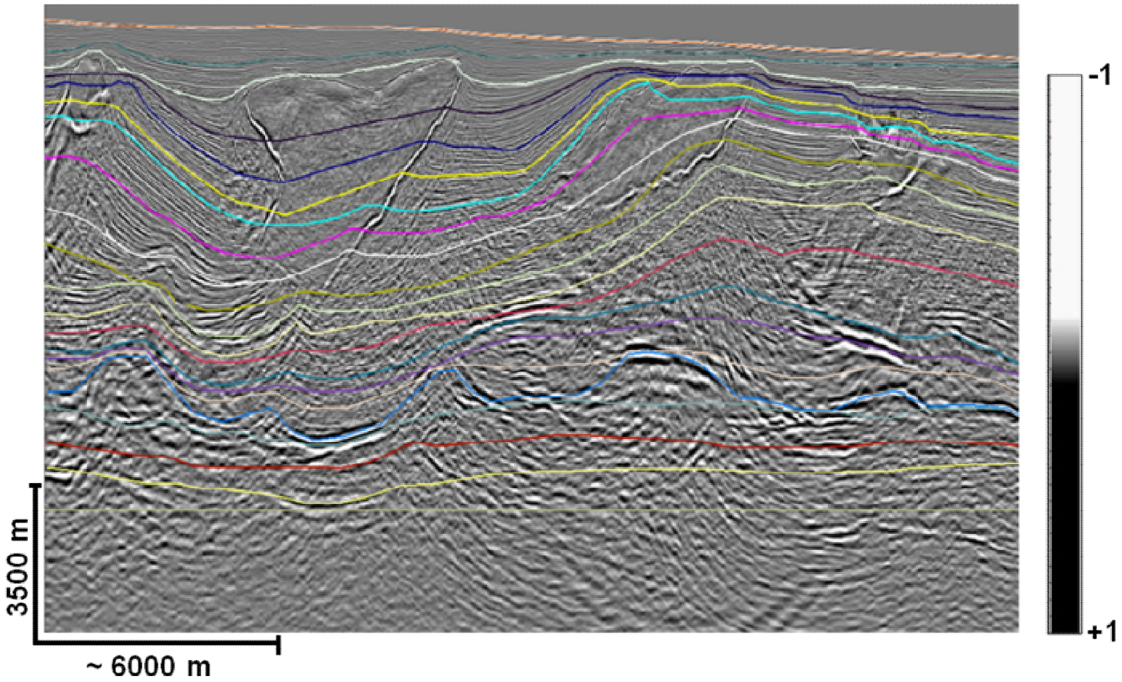

Figure 5.3. Anisotropic Kirchhoff depth migration section with horizon interpretation for 2D finite difference modeling.

The revised velocity model includes a flat horizon at the bottom of the section, as in the Sigsbee model, that helps to study the propagation of the signal through the wavefield and to validate the migration.

Three levels were populated with diffraction points to highlight the maximum dip angle that can be illuminated (see Table 5.2. for parameters).

Diffraction Points Parameters	
Dimensions	dX = dZ = 50 m
Number of points per layer	23
Distance between diffraction points	695 m
Depth of the layers	4000 m, 8000 m and 12000 m
Interval velocity of the shallow layer	3750 - 4000 m/s
Interval velocity of the medium and deep layers	4500 m/s

Table 5.2. Diffraction points parameters.

The horizons were inserted in the TGS sediment velocity model using two parameters: the velocity variation with respect to the background sediment velocity and the thickness of the horizon. Table 5.3. shows the horizon-marking parameters used in the velocity model. Salt canopies and the hard layer were later added to build the final velocity model.

Horizon	Notes	Velocity variation respect to the background(%)	Thickness of the layer (m)
0	Water Bottom		
1		-5	50
2		5	50
3		-5	50
4	Shallow	4	60
5		-4	60
6	Medium	4	60
7		-4	60
8	Deep	4	60
9		-3	70
10		3	70
11		-3	70
12		3	80
13		-3	80
14		3	80
15		-3	80
16	TOP HARD LAYER		
17	BASE HARD LAYER		
18		3	90
19		-3	90
20		2	100

Table 5.3. Layer parameters

The reflection interfaces are the result of velocity contrasts, which varies ± 125 m/s relative to the sediment interval velocity. This produces velocity variations strong enough to produce reflections, but insufficient to destroy the basic gradient macro model which is used in depth migration. The thickness of each horizon marker increases with the depth, to account for decreasing resolution.

The parameters of the revised interval velocity model are shown in Table 5.4. , and Figure 5.4. shows the revised model.

Revised Interval Velocity Model Parameters	
Number of velocity traces	4788
Velocity trace increment	10 m
Velocity depth sample	10 m
Total depth of the model	16000 m
Salt interval velocity	4500 m/s
Sediment interval velocity	TGS (resampled from 25m to 10m)
Water bottom	thin layer

Table 5.4. Revised interval velocity model parameters.

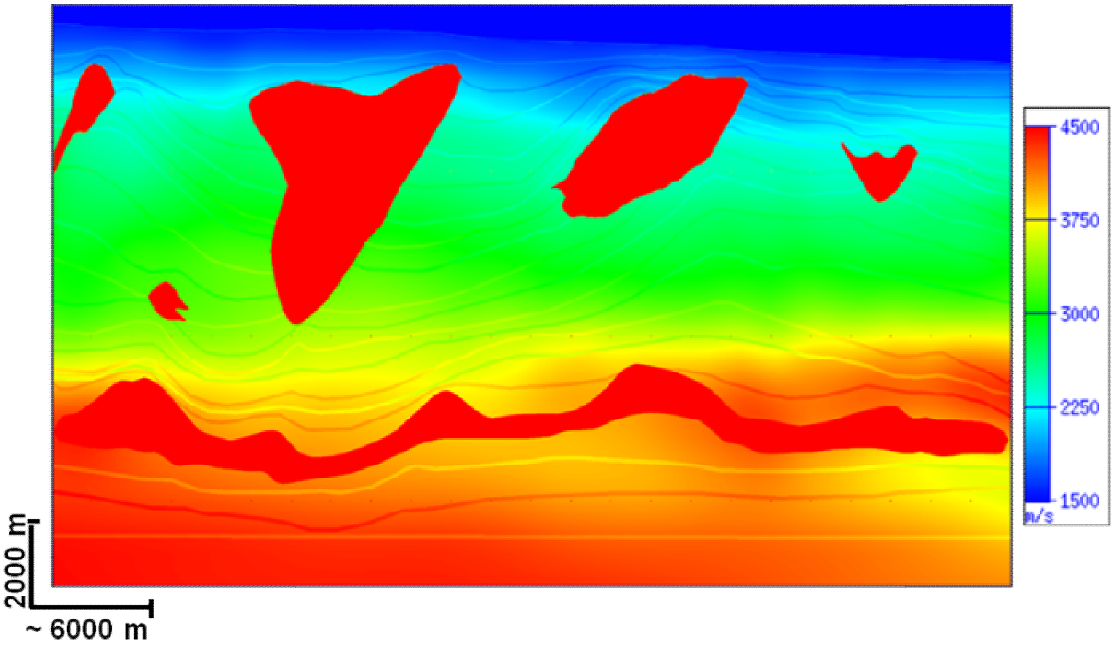

Figure 5.4. Revised interval velocity model

5.3.2. Full wave seismic modeling

The synthetic gathers are computed by Repsol's proprietary finite difference modeling code. The following paragraphs describe the modeling method.

The scalar wave equation in two dimensions (x,z) can be written as:

$$\frac{\partial^2 u}{\partial x^2}+\frac{\partial^2 u}{\partial z^2}=\frac{1}{v^2}\frac{\partial^2 u}{\partial t^2}. \tag{11}$$

Acoustic finite difference method proposes an approximation to the derivatives in the wave equation, by assuming isotropy and constant density. In terms of (x, z, t) grid indices (i, j, k) the finite difference approximation to second order in space and time (Kelly et al., 1976) is:

$$c(i,j) * [60u(i,j,k) - 16[u(i,j,k) + u(i+1,j,k) + u(i,j-1,k) + u(i,j+1,k)] + u(i-2,j,k) + u(i+2,j,k) + u(i,j-2,k) + u(i,j,k)] = u(i,j,k+1) - 2u(i,j,k) - u(i,j,k-1). \tag{12}$$

The method requires the implementation of the following conditions:

1.Stability:

$$\frac{(v_{max} * dt)}{dx} < 0.707, \tag{13}$$

where v_{max} is the maximum interval velocity, dt is the time increment and dx is the horizontal increment.

2. Grid dispersion control:

$$\frac{v_{min}}{(2 * f * dx)} > 6, \tag{14}$$

where v_{min} represents the minimum interval velocity and f is the frequency.

3. All the boundaries of the model are treated as absorbing surfaces.

Selected numerical modeling parameters are given in Table 5.5.

Model Computation Parameters	
Acoustic finite difference (constant density)	
Grid size	dx = dz = 10 m
Dominant frequency	12 Hz (Ricker wavelet)
Single source point	20m receiver array

Table 5.5. Model computation parameters.

The full wave acquisition design attempts to reproduce GEDCO's survey developed in the area (appendix 1). The acquisition parameters of the model appear in Table 5.6.

Acquisition Parameters	
Number of channels/shots	901
Group interval	20 m
Shot interval	100 m
Cable length	18000 m
Receiver interval	20 m
CMP interval	20 m
CDP range	1-4788
Record length	12000 ms
Computing sample length	1 ms
Output sample rate	4 ms
Source	Sea level

Table 5.6. Full wave acquisition parameters.

5.3.3. Snapshot wavefield analysis

The impulse response shows how the wavefront propagates trough the model, highlighting illumination issues.

Table 5.7. shows the parameters that control snapshot wavefield analysis.

Wavefield Snapshot Parameters	
Wavelet	Ricker
Peak frequency	12 Hz
Sample rate	dx = dz = 10 m
Number of samples	nx = 4788, nz = 1601
Time sample rate	dt = 1ms
Number of time samples	nt = 8000
Minimum interval velocity	1500 m/s
Maximum interval velocity	4500 m/s

Table 5.7. Wavefield snapshot parameters.

5.3.4. Synthetic imaging

The shot gathers are migrated after sorting by shot location, resampling every two traces, and muting the direct arrivals. The migration algorithm is reverse time migration, with constant density and isotropic velocity model.

The shots gathers are migrated using two different velocity models. The objective is to evaluate the impact of the velocity model on the migration image. The first velocity model is the one used for the real data migration in the studied line. The second is the modified velocity field with increment velocity markers at each horizon, as described earlier. The names that are used to refer to both models are original and revised velocity, respectively.

The migration parameters are shown in Table 5.8.

Migration Parameters	
Maximum depth	14000 m
Depth interval	10 m
Aperture	12000m: Like in the anisotropic reverse time migration, the aperture is equal to 1.5 offset.
Dominant frequency	12 Hz
The entire model is grided	47880 m x 14000 m

Table 5.8. Migration parameters.

The code used to generate the migration image has been developed by Repsol. The code has two outputs:

- The Hessian matrix, which helps to identify shadow areas. The results of the Hessian Matrix are in Appendix 3.
- The 2D post-stack reverse time migration.

After the migration, both outputs are filtered, eliminating the high frequency content.

Chapter 6

EXPECTED RESULTS

The main objective of this study is to demonstrate that subsalt events are poorly illuminated. The proposed methodology identifies the origin of the shadow areas by calculating the critical angle. Shadow areas are delimitated by 3D ray tracing and validated by 2D full wavefield modeling. The results of both techniques will suggest some solutions to improve seismic data quality and illumination.

The critical angle depends on salt-sediment velocity contrast and relative orientation of the base of salt and the target. The orientation includes both the dip and the azimuth angles. The critical angle can vary along the base of salt, especially when this surface is not flat, and the shape of the stratigraphic target changes from one reflector to the other.

I focus on a subsalt reflector that exhibits a double image. The critical angle evaluates which rays can reach the surface inside the acquisition grid, after hitting the base of salt. The results indicate that some dip angles cannot be illuminated.

From expected values of the critical angle, a 3D computation would obtain a high fold value in the steep dip sediment-terminations since these rays do not intercept salt, and the ray path would be registered inside the acquisition grid. On the other hand, a ray path from a flat sediment layer will travel to the salt body and either bounce back (and then reach the surface out of the grid) or travel through the salt body. In either case, it will be difficult to recover the signal. So, the inclination of the target can affect the ray tracing results.

The depth of the target also influences on the results. The shallow horizon should exhibit higher fold values than the deep horizon.

The delimitation of the shadow zones vary depending on the seismic acquisition design. The offset and azimuth distributions determine the fold value at a certain reflection point. In other words, both the offset and azimuth ranges should be as high as possible.

In theory, wide azimuth acquisition should reduce the poorly illuminated areas compared to narrow azimuth, because the signal recovery increases. The parameters used in wide azimuth acquisition design are represented in Figures 5.2. and 6.1. The offset ranges are 100 – 8000 m in the inline direction and 100 – 4200 m in the crossline direction.

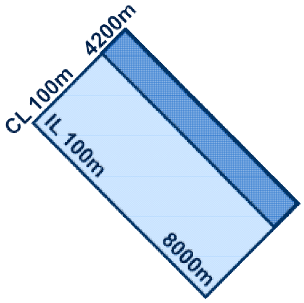

Figure 6.1. Comparison scheme between wide and narrow azimuth acquisition designs. The dark blue rectangle represents the narrow azimuth. The widest rectangle is four times bigger than the narrow azimuth and represents the wide azimuth design.

These parameters are similar to another seismic acquisition survey developed in the studied area.

The full-azimuth design is added in the illumination study as a third survey type. Full-azimuth acquisition represents the best case scenario (Figure 5.2A). It is an ideal design that includes, in our case, every offset between 100m-8000m in the in-line and cross-line directions. If full azimuth shooting has shadow areas, it means the image quality cannot be improved by increasing the azimuth range.

The analysis of the results of the narrow, wide, and full azimuths illumination study define the boundaries of the shadow areas, illustrate the impact of seismic survey design, suggest ways to increase signal recovery at the surface and subsalt illumination.

Fold maps are generated for the different horizons (with narrow/wide/full azimuth seismic acquisition), and ray paths are displayed at the horizon terminations against salt as quality control. Displayed rays are divided in near (0^o-15^o) and far angle (15^o-30^o), and analyzed for other clues to improve subsalt illumination.

The last part of the workflow is full wavefield modeling. Considering that 3D ray tracing only simulates the ray path from the horizon to the surface, it is necessary to simulate the full-wave equation. The results mirror the previous results as it should. Otherwise the assumptions in ray tracing are not correct. Finally, a revised velocity model is proposed that includes sea floor, shallow, medium, deep, top, and base of salt horizons, among others.

The model also contains a deep flat horizon to study how much energy reaches that level. If that plane is not flat, it means that the migration velocity model is incorrect. In the case that the event is not continuous, it means that part of the energy at that depth is not getting into the receivers inside the aperture.

The shot gathers of the model are migrated using two different interval velocity models. The idea is to test the accuracy of the original velocity model used in the real data migration. For example, subsalt sediments located inside the left ellipse in Figure 3.3., seem to be pulled up by incorrect base of salt. If the base of salt is deeper, then the velocity would increase and the seismic events would move down., making better geological sense.

The Hessian matrix is computed at the same time as the migration (Appendix 3). The results of this technique represent the maximum illumination of the model. If the Hessian Matrix exhibits shadow areas, then the seismic acquisition is not able to eliminate them.

The aperture value is tested by full wavefield modeling, since inclination of the salt flanks reflect the rays further than the 12 km aperture, which is the value used in anisotropic reverse time migration.

Chapter 7

RESULTS

In this chapter, the results of the critical angle estimation, ray tracing and full wavefield modeling confirm that the available dataset exhibit some illumination issues, including subsalt events cannot be visualized in the seismic image.

The critical angle explains the reasons that cause the lack of illumination. The salt flanks are steep dip, closing to the critical angle, making the subsalt layers difficult to illuminate.

7.1. Critical angle analysis

The critical angle relates to the maximum angle that can be illuminated in the seismic image, by applying certain acquisition design to a geological area. This parameter helps to find the origin of the shadow areas.

The angle limit of illumination depends on the inclination of the base of salt, the dip of the sediment against the salt, and the interval velocities of the sediment and the salt (Snell’s law). Figure 7.1. shows an area where subsalt illumination is limited to dips less than 1 degree ($\theta_d = 1°$). The values shown in Figure 7.1. only represents one reflector point and cannot be extrapolated to the rest of the seismic section because the angle limit of illumination changes depending on the previous mentioned parameters.

The low dip termination ($\theta_{target} = 1.28°$) has an angle greater than the maximum imaging dip angle, so the subsalt flat events cannot be illuminated and thus define a shadow area. The base of salt has a dip angle closer to the critical angle (dash line). Muerdter and Ratcliff (2001) show that the subsalt sediments have a limited illumination when the inclination of the salt flank is closer to the critical angle.

Therefore, these results demonstrate that the shadow zones are caused by both relative orientation of the strata with respect to the salt structure and the velocity contrast at the salt-sediment interface. Rays that reach the surface successfully are from targets with an inclination lower than the maximum imaging dip angle.

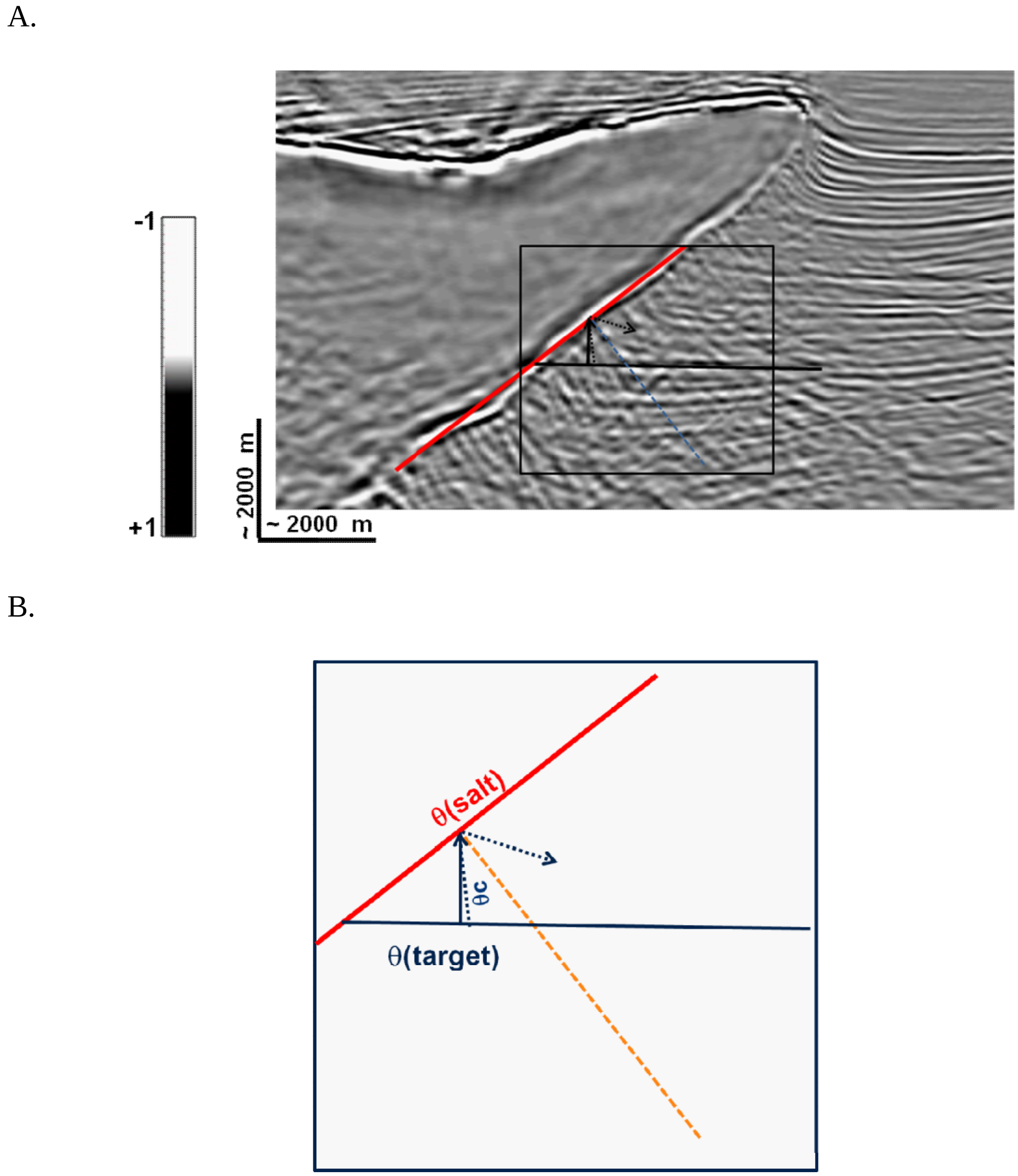

θ(target) = 1.28° θ(salt) = 37°

sin θc = vlayer/vsalt = 2800/4500 θc = 38°

θd= 38 ° – 37 °= 1° (maximum imaging dip at target)

θ(layer) = 1.28° > 1° Closer to the max. imaging dip-angle. **It cannot be illuminated**

Figure 7.1. Details of Snell's law calculation to determine illumination. A. Anisotropic reverse time migration with critical angle calculation. B. Details of critical angle calculation.

7.2. Horizon interpretation

The chosen horizons represent three sediment layers with increasing depth they are termed shallow, medium, and deep. Anisotropic reverse time migration and anisotropic Kirchhoff depth migration volumes were used in the horizon definition. The picked horizons are represented in Figure 7.2., showing depth, dip, and azimuth for each.

The main objective of the interpretation is to demonstrate the limits of seismic illumination. For that reason, the terminations of the sediment layers against the salt-bodies have been picked flat where the quality of the image is poor. In Figure 7.2., the flat areas are characterized by separate depth-contour levels and are represented by blue color in the dip maps.

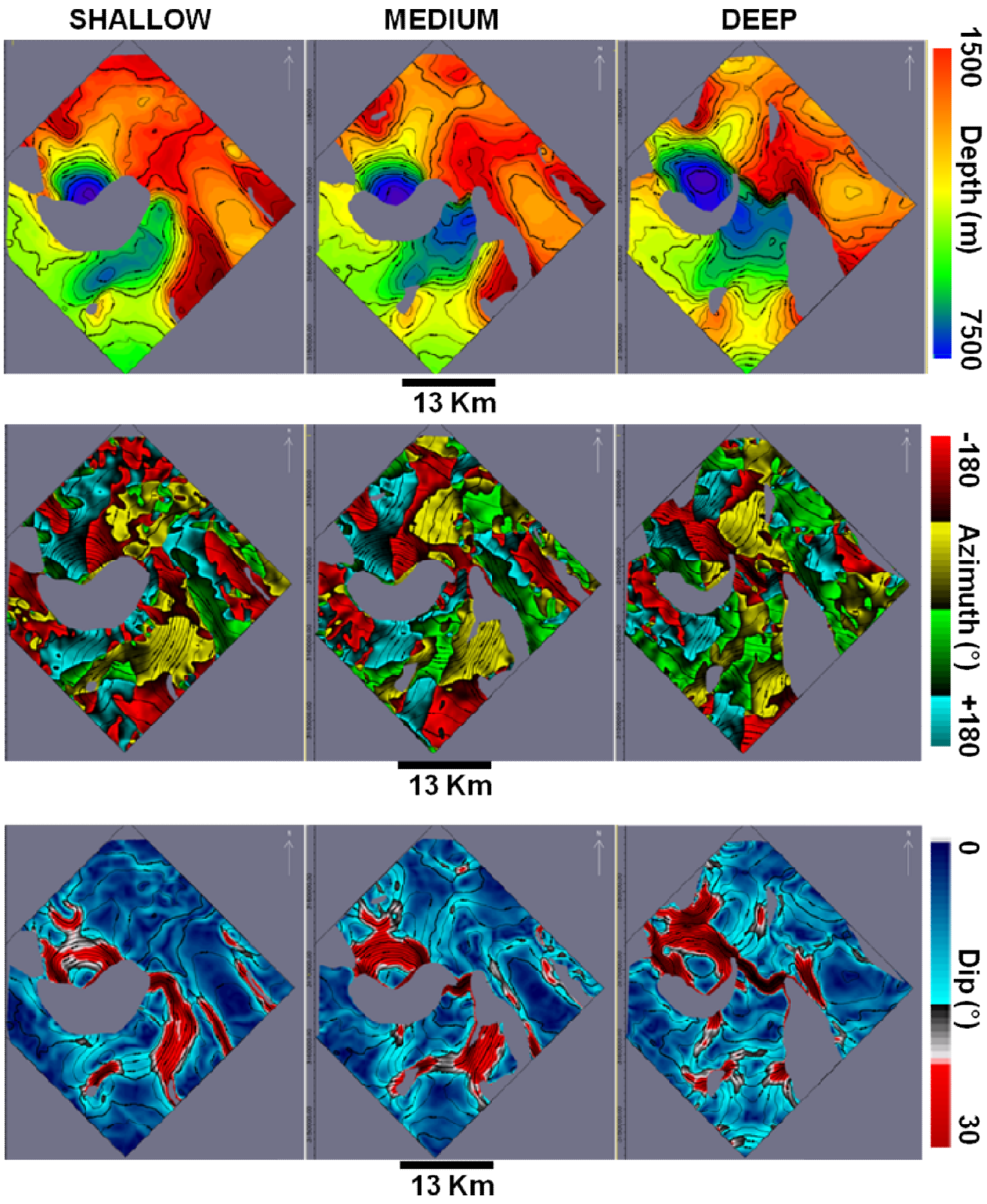

Figure 7.2. Interpreted horizons from left to right: shallow, medium and deep. (upper) Depth contour maps. (middle) Azimuth maps with depth contours. (lower) Dip maps with depth contours.

7.3. Ray tracing

Ray tracing defines the limit of the poorly illuminated areas, depending on acquisition design. Epos 3 ray tracing software was used, and it is assumed the TGS velocity model is correct, the earth is isotropic and the ray path travels one-way from the target to the acquisition surface. The results also depend on the geological model, interval velocity and shape of the target.

The shadow zones are determined by the dip-azimuth relation between the salt structure and the stratigraphic layers, and the velocity contrast between both lithologies, as well as the distribution of azimuth and offset in the seismic acquisition.

Three different acquisition designs are considered, all shooting 45° NW - SE:

1. Narrow azimuth: inline range: 100 m – 8000 m and crossline range: 100 m - 1000 m. The available data was acquired using this design.

2. Wide azimuth: inline range: 100 m – 8000 m and crossline range: 100 m – 4200 m. These parameters are based on a future seismic survey.

3. Full azimuth: inline range: 100 m – 8000 m and crossline range: 100 m - 8000 m. This is an ideal case and represents the maximum azimuth recovery.

7.3.1. Narrow azimuth seismic acquisition

The field data was shot with a narrow azimuth as described by parameters in Appendix 1. The results of 3D ray tracing for this design is shown in Figure 7.3.

Each fold map is computed independently.

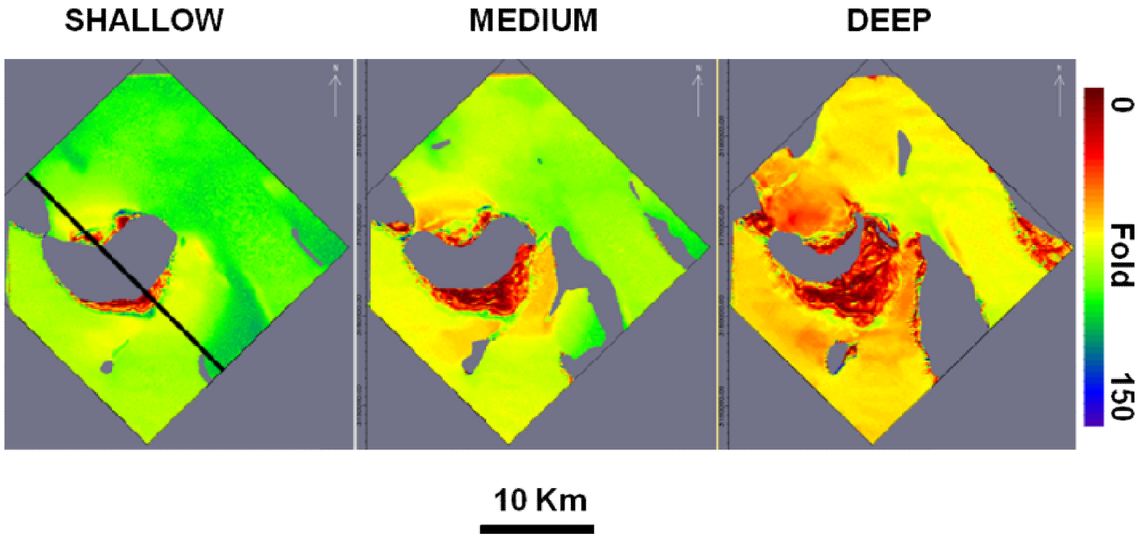

Figure 7.3. Narrow azimuth acquisition illumination results from 3D ray tracing. Red is poor illumination. The black line represents the seismic section of interest.

The results show that the shallow surface has better illumination (fold > 100) than the deep surface (fold < 80). This agrees with the seismic section (Figure 7.4.), where the quality of the image is better at the shallow level.

The defocusing areas are perfectly defined in dark red, where the fold values are smaller than 15. Those poorly illuminated areas increase progressively with depth, associated with the shape and orientation of the base of salt. In Figure 7.3., the low fold areas (in red) match with the poor quality image zones in the seismic of Figure 7.4.

Note the distance between the shadow zones caused by the two main salt bodies is 5 km at the deeper horizon. That distance is smaller than the maximum in-line offset (8 km).

The subsalt shadow zones correlate with the low dip values at the three different levels, matching the theory that maximum illumination angle is determined by the critical angle, which depends on V_p velocity ratio between the salt and the sediment, and the salt structure orientation. If the strata terminations against the salt body are lower (flatter in this case) than the critical angle, then the sediments are not illuminated generating a shadow zone.

The shadow zones are surrounded by high fold values. The energy is focused on those areas, so the number of rays recovered at the surface inside the acquisition grid is much higher than the defocusing areas.

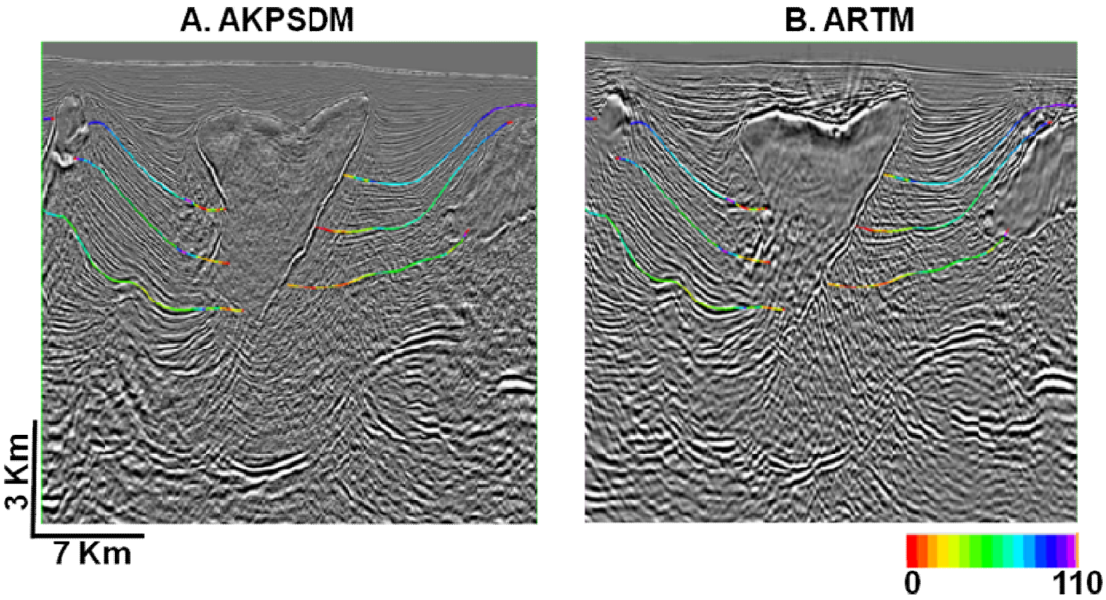

Figure 7.4. Illumination results of 3D ray tracing with narrow azimuth acquisition geometry over the three studied levels. Comparison results with the A. anisotropic Kirchhoff depth migration and B. anisotropic reverse time migration volumes.

The high amplitude areas shown in Figure 7.4., coincide with the highest fold values in green-blue for the different events. These zones are generated by the focusing of the energy of the rays between the salt structures, hitting those sectors more.

Figure 7.5. shows the ray tracing results based on the deep horizon, comparing a seismic line of the anisotropic reverse time migration with the ray path at certain location with a fold value closer to zero. The poor image of the seismic line is located where the fold values are lower than 15 (orange to red).

It is important to display the ray path at certain locations to understand the ray tracing results. In Figure 7.5., the ray paths are displayed over the horizon map, thereby showing if the rays are recovered inside the seismic acquisition grid (blue rectangle).

Blue rays represent the energy that cannot be recovered at that location. The rest of the possible ray paths appear in magenta. The rays that travel through the salt cannot be recorded at the surface, so those are considered lost data.

The rays are divided in the following ranges:

- Full: dip angle: 0° to 30°, and azimuth: -45° to -44°.
- Near: dip angle: 0° to 15°, and azimuth: -45° to -44°.
- Far: dip angle: 15° to 30°, and azimuth: -45° to -44°.

The full shooting dip angle case shows a zero-fold value. In other words, there are no rays hitting the grid area (8 km by 1 km), represented by a blue rectangle in Figure 7.5. The incident rays travel through the sediment events, from the deep horizon to the salt body. Then the rays are either:

- bounced back,

- deviated and recovered out of the seismic cell, or
- forced to travel through the salt body,

In the near angle case, which is equivalent to the near offset, every ray is deviated out of the acquisition area. Both the azimuth and the offset of the rays are higher than the acquisition parameters.

The far angle, which can be correlated with far offset, does not pick any ray inside the acquisition grid. As expected, the far offset is less affected by the salt edge than the near (Muerdter and Ratcliff, 2001). In this case, the ray paths could be recovered by acquisition offset longer than 8 km.

A. Full shooting dip angle

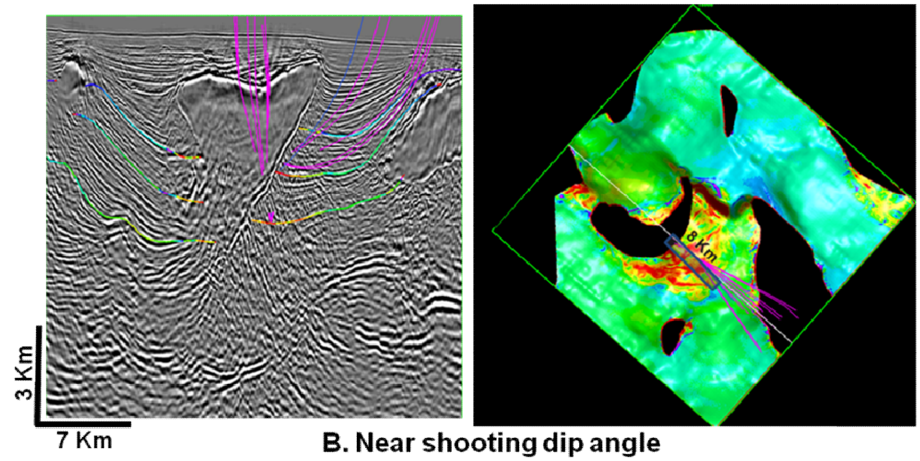

B. Near shooting dip angle

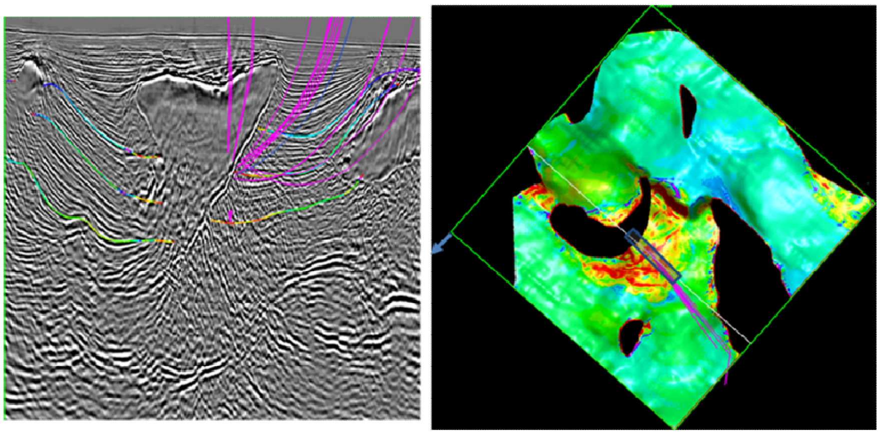

C. Far shooting dip angle

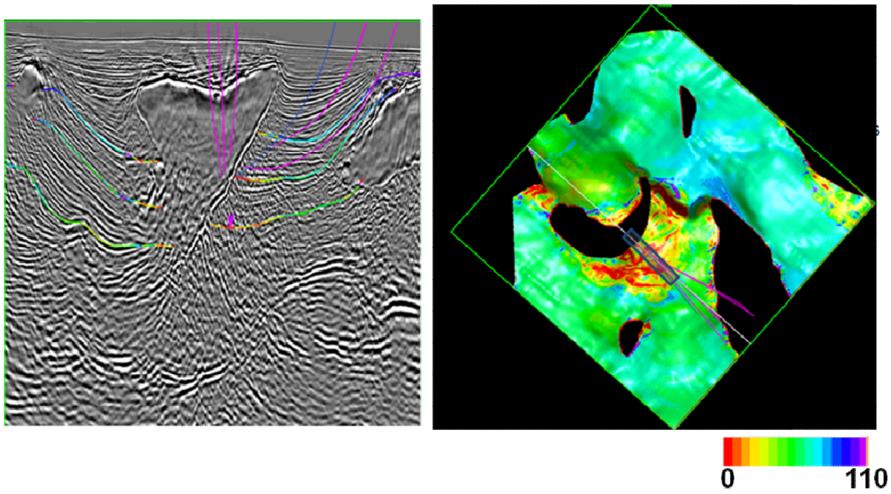

Figure 7.5. Narrow azimuth ray tracing display for deep horizon. A. Full shooting dip angle. B. Near shooting dip angle. C. Far shooting dip angle.

7.3.2. Wide azimuth seismic acquisition

Wide azimuth acquisition could be a solution to improve signal recovery. This design is based on a proposed seismic acquisition design developed in the area, altough there is no seismic data available with this design. The in-line offset range does not change comparing to narrow azimuth, and the cross-line offset range increasing to 100 – 4200 m.

As in the narrow azimuth design, the ray tracing results have been computed independently. The seismic line of interest is highlighted in black in Figure 7.6..

The illumination analysis shows consistent results between the three horizons: shallow, medium, and deep. The fold values are smaller with increasing depth. Compared to narrow azimuth acquisition results the fold values increase (Figure 7.6.).. The mean values are 110, 110, and 90 for shallow, medium, and deep horizons respectively. The subsalt shadow defined by fold values closer to zero, is reduced but not eliminated. The salt wedge still distorts the signal, receiving just a few rays at the surface inside the acquisition grid. The focusing areas around the salt wedge are greater, and have higher values than the narrow azimuth case (fold > 150). This fact could be a potential problem for interpreters since the high amplitude values could be misinterpreted as high acoustic impedance contrast or correlated with a different high amplitude event.

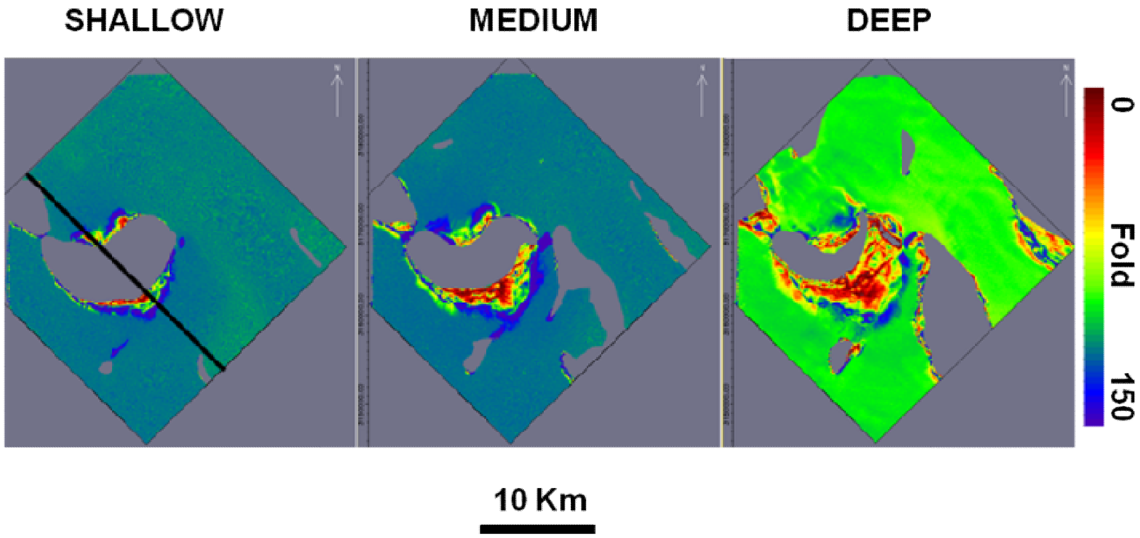

Figure 7.6. Wide azimuth acquisition illumination results. Red is poor illumination. The black line represents the seismic section of interest.

Figure 7.7. shows where the anisotropic Kirchhoff pre-stack depth migration and anisotropic reverse time migration volumes can be improved using a wide azimuth acquisition design. Those volumes were actually acquired with a narrow azimuth design. Even with wide azimuth, the shadow zones still appear in the sediments layers, showing poorly illuminated areas consistent with the dip and azimuth of the base of salt.

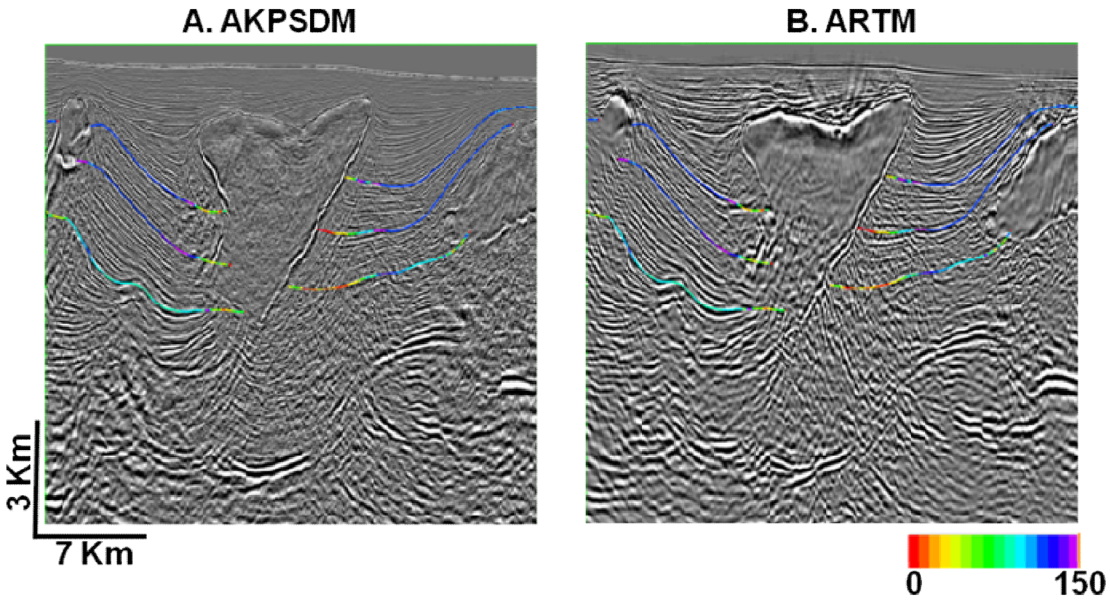

Figure 7.7. Illumination results of 3D ray tracing with wide azimuth acquisition geometry over the three studied levels. Comparison results with the: A. anisotropic Kirchhoff depth migration and B. anisotropic reverse time migration volumes; based on narrow azimuth acquisition.

As in the narrow azimuth case, it is important to study the recovery of signal at the surface using a range of shooting angles (Figure 7.8.). In order to make a fair comparison, the calculations have been completed at the same reflection point shown in Figure 7.5.

The rays are highly dispersed after the full offset shooting. The rays reach the surface following two different trends: traveling through the salt body or reflecting off the wedge and deviating farther than 8 km offset.

The far offset recovers a small portion of the signal inside the acquisition grid (blue rectangle), but the near offset cannot recover any signal inside the acquisition cell, again showing that far offset is less affected by the salt wedge than near offset.

The distance between the disrupting areas is still smaller than the maximum design offset. If the separation between canopies were greater than 8 km, then the subsalt shadow zone would be reduced.

A. Full shooting dip angle

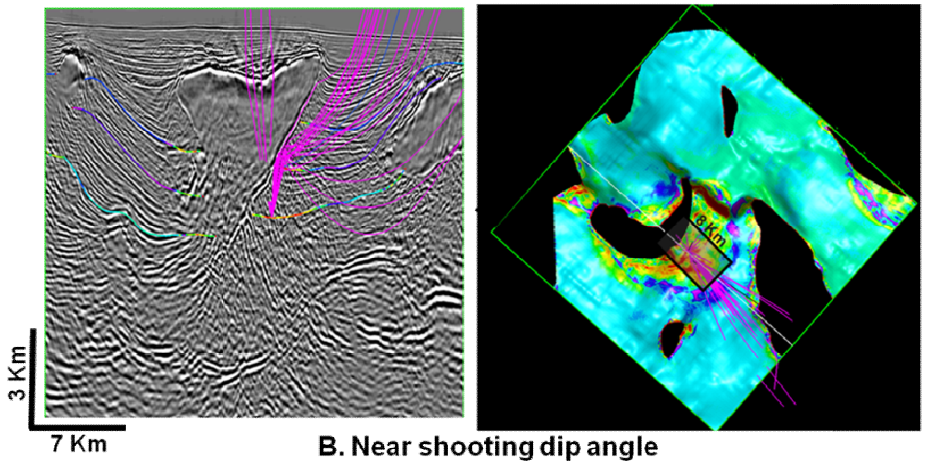

B. Near shooting dip angle

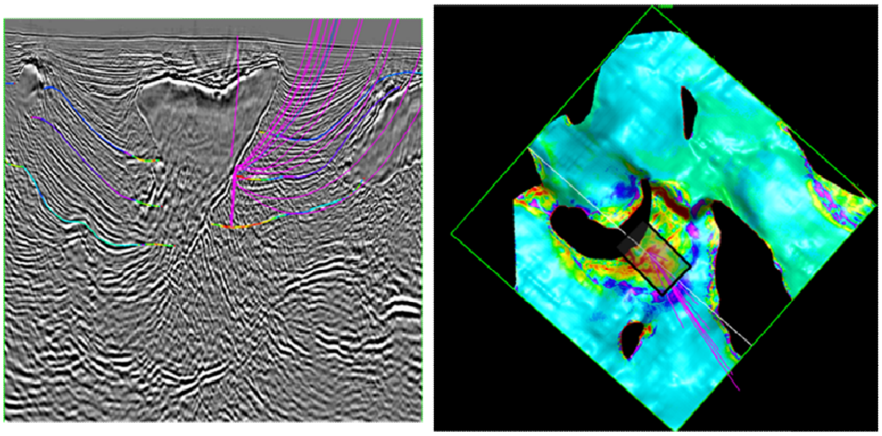

C. Far shooting dip angle

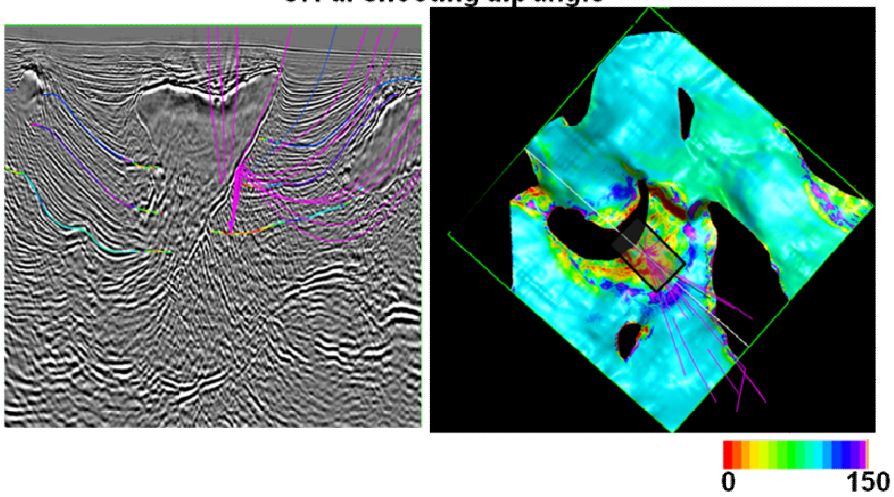

Figure 7.8. Wide azimuth ray tracing display for deep horizon. A. Full shooting dip angle. B. Near shooting dip angle. C. Far shooting dip angle.

7.3.3. Full azimuth seismic acquisition

Full azimuth design represents the ideal case where every azimuth is represented in the seismic acquisition (Figure 5.2A.), with maximum offset 8 km in both inline and cross-line directions. Full azimuth design allows estimation of the maximum fold that can be recorded.

The average fold of the three different horizons reaches a value greater than 300 (Figure 7.9.). The black line represents the studied seismic section and the fold maps have been calculated one at a time. The shadow zones are greatly reduced at all horizons, but there are still some areas where the fold values are close to zero, showing illumination problems for even the best case scenario.

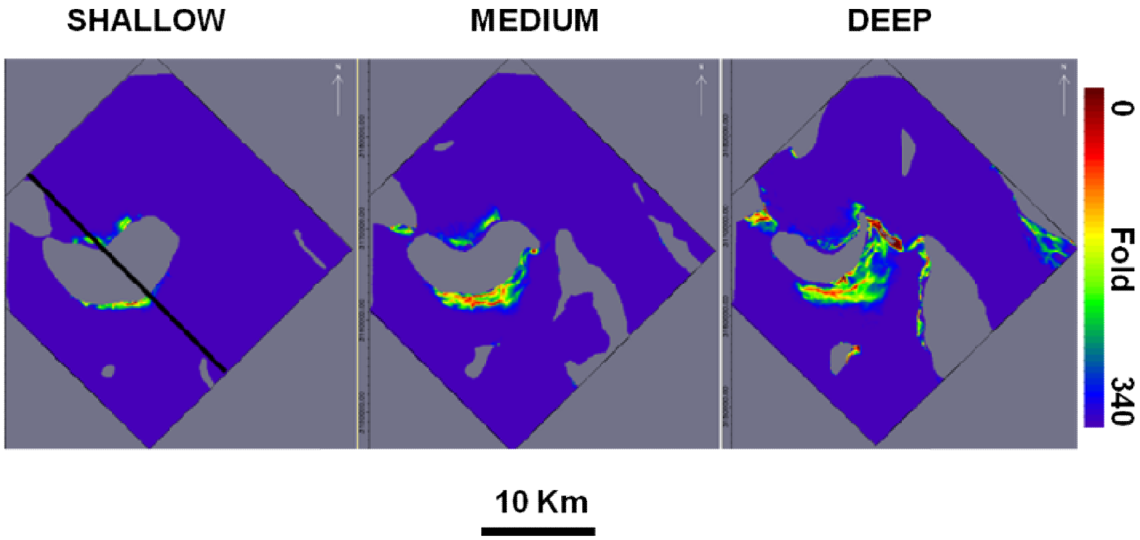

Figure 7.9. Full azimuth acquisition illumination results. The black line represents the seismic section of interest.

Figure 7.10. compares the quality of both seismic images acquired with narrow azimuth using two different migration algorithms, and the ray tracing fold with full azimuth acquisition based for all three horizons. Clearly, a full azimuth design would improve quality of the seismic image independent of the migration algorithm. In this particular section, the fold values would be all greater than 40.

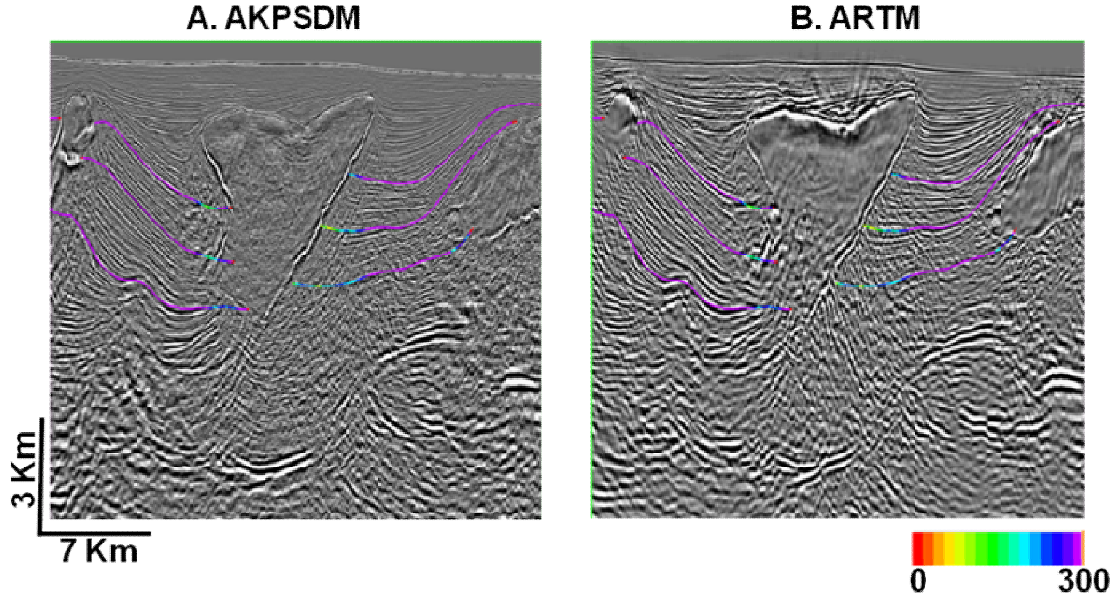

Figure 7.10. Illumination results of 3D ray tracing with full azimuth acquisition geometry over the three studied levels. Comparison results with the: A. anisotropic Kirchhoff depth migration and B. anisotropic reverse time migration volumes; based on narrow azimuth acquisition.

As a means of quality control, full azimuth rays are compared with the ray paths coming from the deep horizon to the surface. Figure 7.11. shows the full azimuth results and the different ray paths for the same common reflection point used in both narrow and wide azimuths.

The first observation of the full azimuth results is the presence of high fold values, showing full azimuth design recovers more rays inside both the acquisition grid than the other cases.

Full azimuth design recover more rays in both near and far offsets than the previous designs.

It is necessary to use longer offsets than 8 km in order to recover more rays inside the acquisition grid.

A. Full shooting dip angle

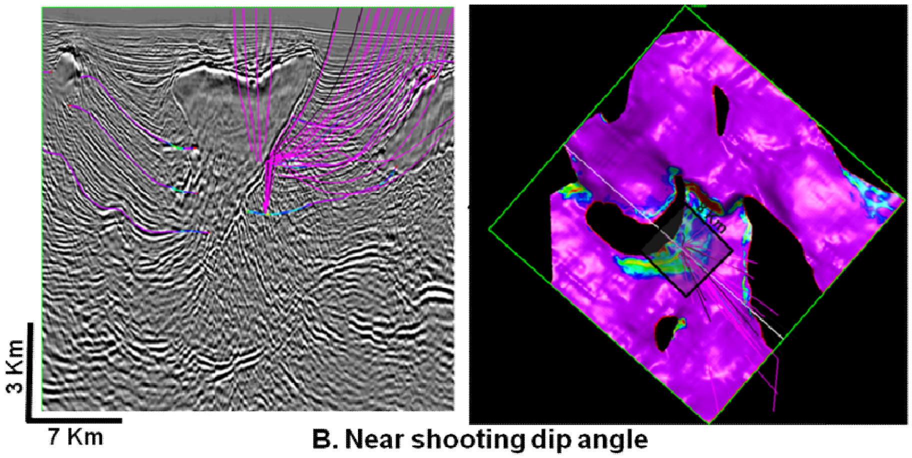

B. Near shooting dip angle

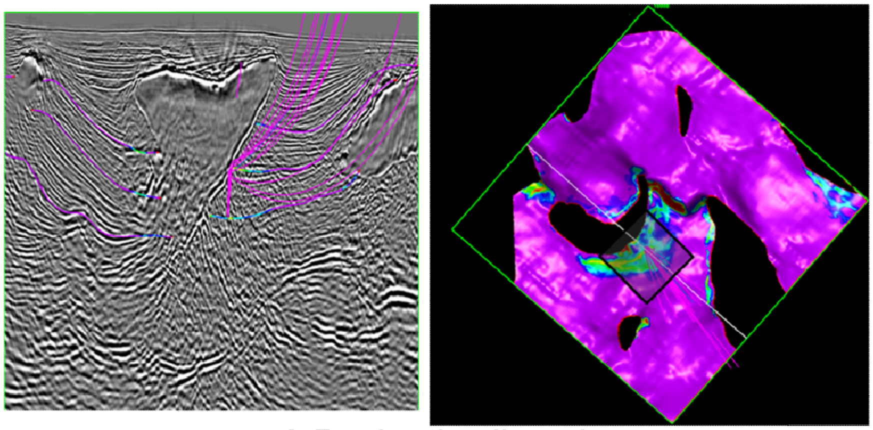

C. Far shooting dip angle

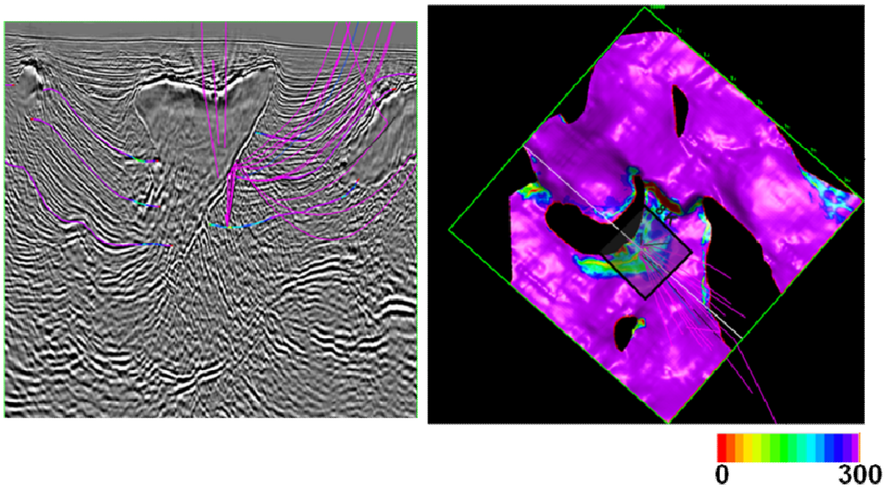

Figure 7.11. Full azimuth ray tracing display for deep horizon. A. Full shooting dip angle. B. Near shooting dip angle. C. Far shooting dip angle.

7.3.4. Summary of ray tracing results

The main objective of this study is to demonstrate that poor seismic quality is due to a lack of illumination. I expect that acquisition design directly impacts illumination results.

From the analysis described earlier, I find both the extent and fold value of shadow areas decrease with the increasing azimuth coverage.

Focusing areas are eliminated with the full azimuth.

The minimum distance between the biggest salt canopies is smaller than the maximum offset, which sets a limitation on illumination improvement, since the salt wedge disrupts every ray that travels in a distance smaller than one half of the offset (Muerdter and Ratcliff, 2001).

Generally, the near offset travels from subsalt horizons to the base of salt and reflects. In the narrow azimuth case, the acquisition grid does not register any signal. The wide azimuth recovers more rays, and the full azimuth improves is even better.

At far offset, the number of rays recovered at the surface increases with the azimuth range.

in all three different survey designs the far offsets recover more rays than the near offsets at the surface inside the acquisition grid, and the far offset is less affected by shape of the base of salt in agreement with Muerdter and Ratcliff (2001).

It is necessary to use an offset longer than 8 km to improve the signal recovery, since the dip of the base of salt deviates rays shooting from the subsurface further than 8 km.

7.4. Full wavefield modeling analysis

The seismic image depends on acquisition geometry as well as the geological model, the velocity, the anisotropy, and the migration algorithm.

The TGS velocity model is an estimation of reality, and the bottom part of the model (Figure 3.1.) is an extrapolation of the velocity. It seems to consider no changes the lithology which cause important acoustic impedance contrasts. However, the anisotropic Kirchhoff depth migration and anisotropic reverse time migration images (Figures 5 and 6), imply there is a hard layer that should be included in the velocity model.

Observing the migration images, the base of salt body located in the middle of the image seems too sharp and does not have any geological explanation, and apparent stratification of seismic events situated underneath could be pulled up by an incorrect velocity model.

Full wavefield modeling helps to understand imaging and illumination issues. Therefore, this study includes a 2D model and full wave simulation that tests some assumptions related with both the velocity model and the target interpretation. Analysis of the results exhibit some solutions to reduce the imaging issues.

7.4.1. Snapshot wavefield analysis

A wavefield snapshot (Figure 7.12.) illustrates complicated wavefront propagation, especially when the wave is traveling through salt bodies. The source is located between CDPs 24 and 25, at sea level. It is represented by a red star in Figure

7.12. The receivers are represented by discontinuous blue line. In overhangs areas, the wave travels faster through the salt than through the sediments, and the wavefront arrives first to the sediments passing by the salt. This fact generates illumination issues that cannot be resolved by migration. The steep dip base of salt shows similar issues.

Both the rugosity of the base of salt and the overhangs act like diffraction points for the wavefront, and the hard layer strongly reflects the wavefront with signal recovery much better from the top.

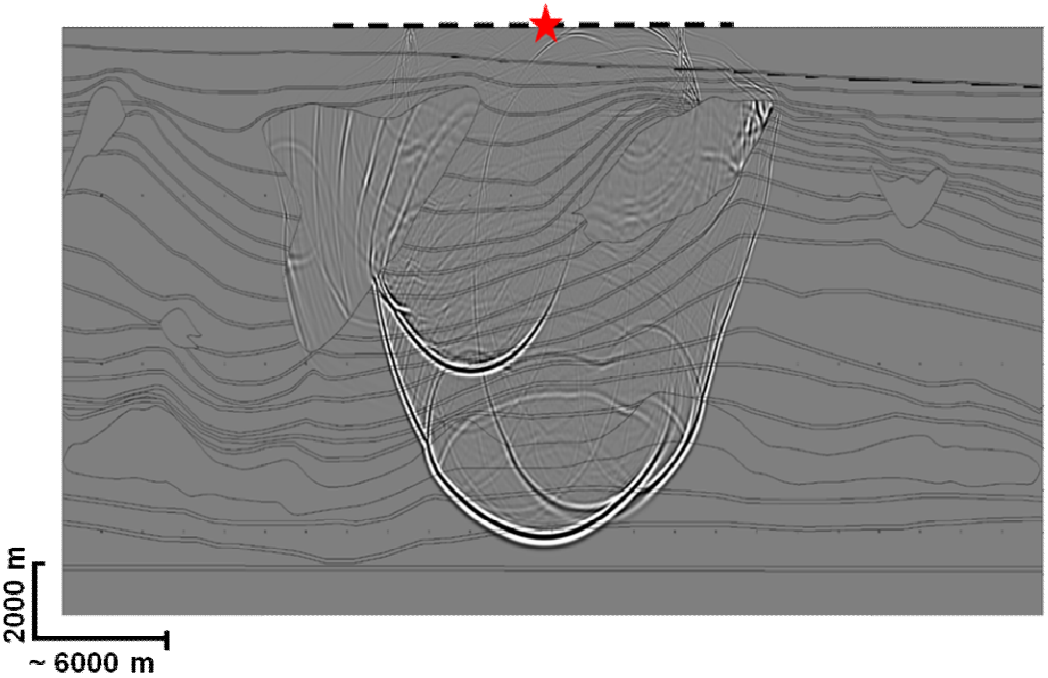

Figure 7.12. 2D acoustic wave simulation impulse response.

7.4.2. Reverse time migration results

Full wave synthetic pre-stack data was migrated to create seismic images using two different velocity models (revised and original). The results are shown in Figure 7.13., where seismic image (A) is migrated with the revised velocity model and (B) with the original model.

The subsalt sediment layers show a decrease in the amplitude in both images, including the deep horizontal event. This dimming coincides with the shadow areas defined by ray tracing.

In the poorly illuminated zones, the diffraction points are not well collapsed. The diffraction points are in the correct position when they are circular indicating every angle can be illuminated. Diffraction points in subsalt areas are elliptical highlighting the maximum illumination dip.

In the first image, the red arrow is pointing to subsalt event terminations that are misplaced, some of them showing a double image. The yellow triangles highlight focusing areas, where the seismic amplitude of the events is abnormally higher. The shadow areas are characterized by a dimming in the amplitude of the seismic events and poor focusing of the subsalt diffraction points.

Figure 7.13.B shows migration of the synthetic data the original velocity model application. It exhibits the same issues as the revised migrated result, including shadow and focus areas, uncollapsed subsalt diffraction points, discontinuous sediment terminations against salt, and false steep dip planes (red arrow).

The incorrect velocity model has a negative impact on the seismic image. It migrates the local events to the wrong position and generates apparent structures that do not appear in the original model. Subsalt sediments located under the main canopy are pulled up, deformed and distorted (red ellipse), and the deep reference horizon is not horizontal.

The blue circle marks an apparent event with high amplitude resulting from incorrect interpretation of salt geometry.

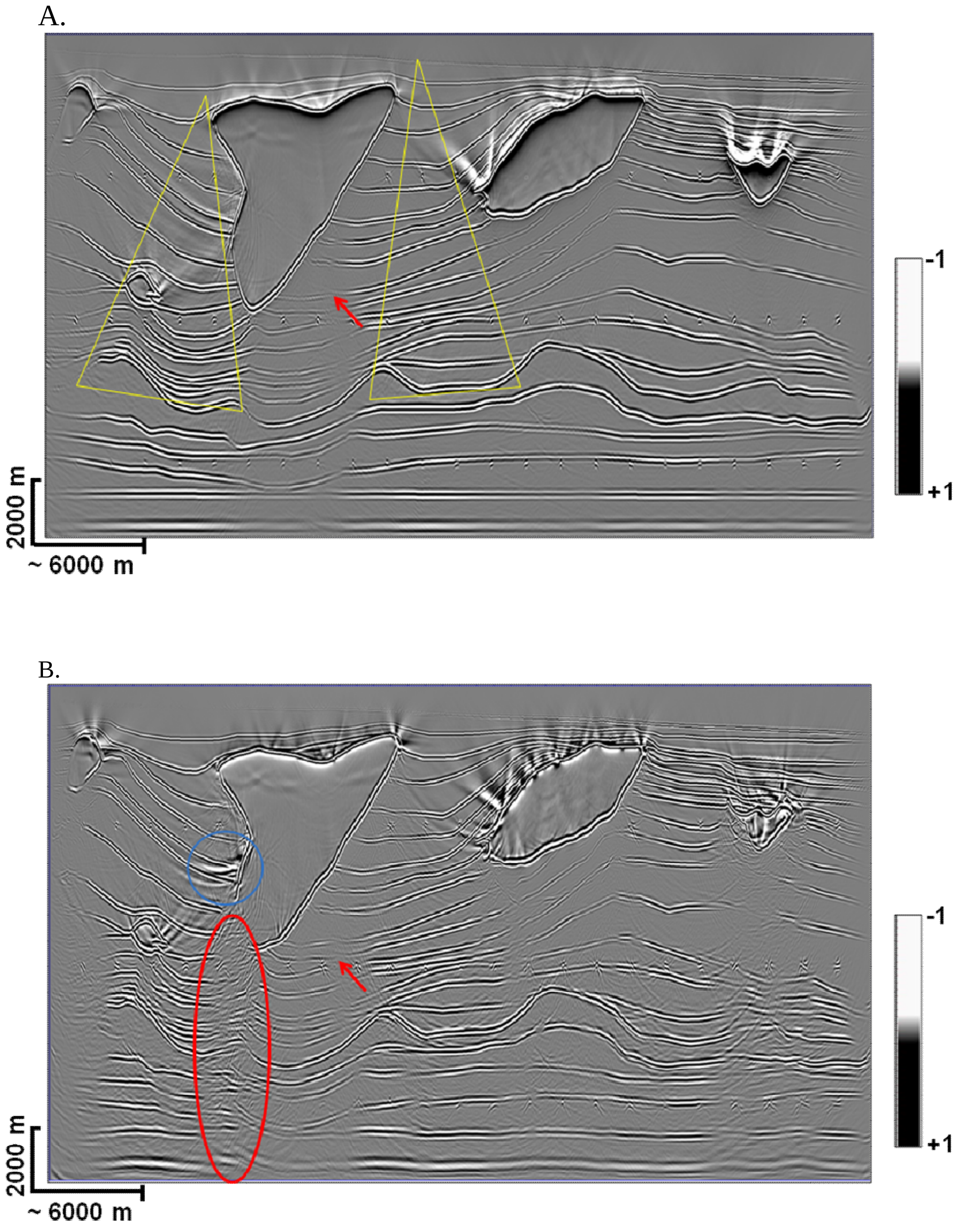

Figure 7.13. Reverse time migration results: A. with revised interval velocity, B. with original velocity model. Highlight areas discussed in text.

7.4.3. Comparison with previous results

Ray tracing simulates one-way travelling from the referenced horizon to the surface. On the other hand, reverse time migration computes the signal path from surface to the reflection point and from the reflection point to surface.

The results of the two different techniques agree on:

1. A steep dip base of salt generates poorly illuminated areas that can be identified by amplitude dimming of events in full wavefield modeling. The rugosity of the flanks distorts the ray paths and reduces the illumination capacity.

2. The focusing areas are located between the salt bodies and are characterized by high amplitude values in the synthetic imaging of the synthetic full wavefield data. Ray tracing results indicate high fold zones surround the shadow areas.

3. The offset used in the seismic acquisition is not long enough to recover rays coming from the subsalt reflectors.

7.5. Comparison with seismic data

Although ray tracing and reverse time migration of the synthetic gathers are computed with an isotropic velocity model, they obtain equivalent illumination results to the anisotropic reverse time migration section (Figure 7.14.).

Extent of the shadow areas correlates with the salt flanks. Both the shape and the dimensions depend on the rugosity and the inclination of the base of salt, as well as orientation of the sediments terminations, and subsalt events exhibit a dimming in the amplitude.

The focusing areas are located between the salt bodies (yellow triangle), where the signal recovery is higher. Also, the high fold zones delineate the poorly illuminated sectors. The amplitude values are abnormally high.

The maximum illumination dip is indicated by subsalt diffraction points that cannot be reconstructed by reverse time migration, whose elliptical shape indicative of the orientation of the ray paths that can be recovered at the surface.

Terminations against the salt are discontinuous and subsalt seismic events have a double image (highlighted with red arrows in Figure 7.14.).

The picking of the base of salt should be reviewed. Since synthetic imaging confirms that the incorrect velocity model can generate false structures and distort the image. The red ellipse contains similar discontinuities as seen in Figure 7.13.B.

The presence of a deep hard layer in the real data section is possible. As shown in full waveform modeling, it is difficult to recover the signal coming from reflectors under the hard layer. The picking of this layer should be flatter than the model (Figure 5.3.), because this event is deformed by the salt bodies. Also, energy focusing highlights different geological events, equalizing the apparent amplitude and complicating the interpretation of that particular layer.

In Figure 7.14., the circled area in blue exhibits comparable illumination limits as in the synthetic imaging caused by a salt overhang.

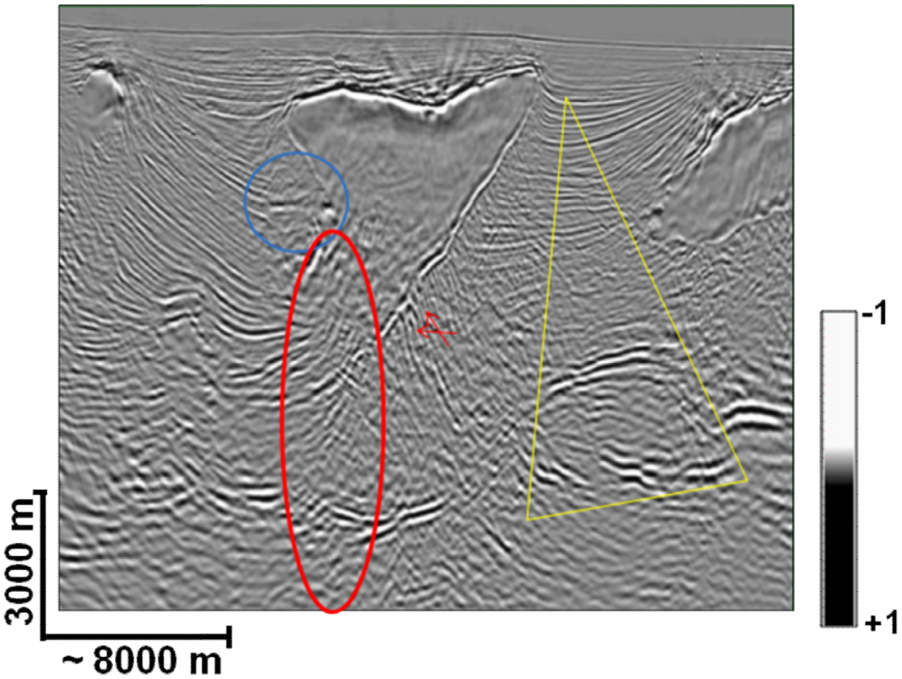

Figure 7.14. Anisotropic reverse time migration section. Highlight areas analyzed in text.

Chapter 8

ADDITIONAL ANALYSIS

Chapter 7 explains the reasons behind the lack of illumination and defines the boundaries of the shadow areas. At the end of the chapter, the possibility to improve the seismic image using two different acquisition designs that have the same shooting direction NW-SE is suggested.

In order to improve the quality of the image, this chapter will study the impact of additional ideas that affect the illumination of the seismic events.

The first idea is that shooting direction, more specifically, the impact of the quality of the seismic when the signal is shooting in a direction perpendicular to the original data.

The second idea is that migration aperture can be tested using the 2D model.

8.1. Shooting direction

The ray tracing study demonstrates that the quality of the seismic image improves when the azimuth range increases. Nevertheless, this parameter cannot resolve all illumination issues by itself.

The previous analysis assumes the actual seismic acquisition direction 45°NW-SE. The available dataset is a small part of a much larger survey, so the parameters of the survey were not designed to focus on the area of interest. As a result, it is reasonable to check if the actual shooting direction is optimum.

Ray tracing has been recomputed over the deep horizon, with a shooting direction perpendicular to the actual one, so that the inline direction becomes the crossline, and vice versa. This test orientation was chosen since the 45° SW-NE direction is the most extreme case (orthogonal to actual shooting direction).

The new acquisitions designs considered in the ray tracing study are:

- Narrow azimuth: inline offset range: 100 - 8,000 m and crossline offset range 100 - 1,000 m,
- Wide azimuth: inline offset range: 100 - 8,000 m and crossline offset range 100 - 4,200 m.

Figure 8.1. shows compares ray tracing results over the deep horizon, for narrow and wide azimuth with the two perpendicular shooting directions. The full azimuth acquisition is the same in both directions. Each fold map has the same color palette. The dark blue indicates zero fold and the red color indicates fold values equal or higher than 240.

The differences between the two shooting directions are not significant in the narrow azimuth results. In fact, the shadow and focusing areas slightly increase. Also, wide azimuth results show smaller differences that will not improve the quality of the image.

In conclusion, the modification of the shooting direction does not significantly affect the results. This alternative is not a solution for illumination issues in this setting.

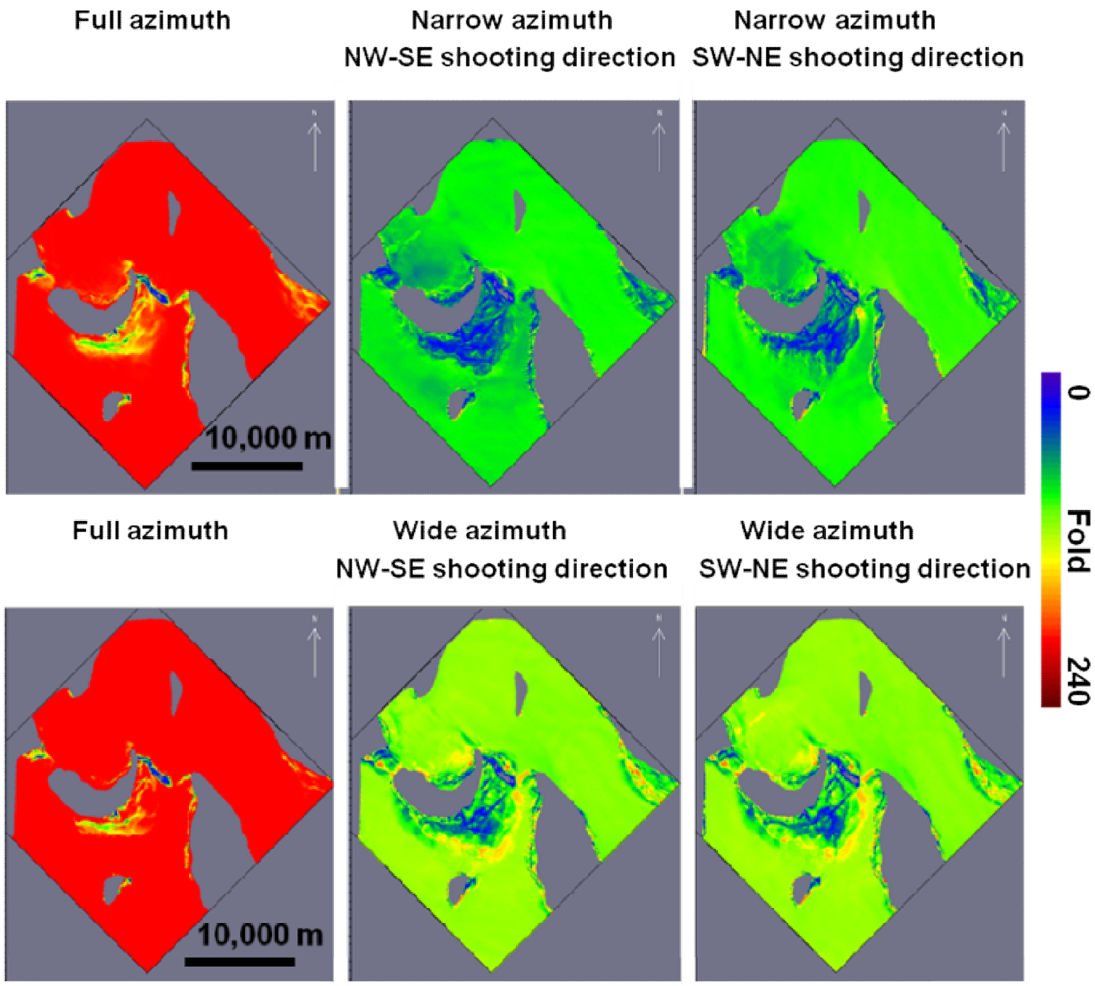

Figure 8.1. Narrow and wide azimuth ray tracing results with perpendicular shooting directions.

8.2. Aperture analysis

Migration aperture is an important parameter that affects the seismic image. In order to study the aperture effect on the migration results, the synthetic gathers generated by the full wavefield modeling are migrated again using both velocity models with the following aperture limits: 4 km, 8 km, and 20 km.

Figure 8.2. exhibits the reverse time migration images migrated with 20 km aperture. The upper image uses the revised velocity model and the lower image is generated with the original velocity model.

The subsalt sediments exhibit a better image than in Figure 7.14. (where the migration aperture was 12 km), as the continuity of the events improves markedly. The double image of the strata terminations against the salt almost disappears (see black ellipse). Even in the migrated image using the original velocity model, the termination trends match the input model. This implies the 12 km aperture used in the field seismic data migration could generate a double image at the salt-sediment interface.

Also, shadow areas decrease, diffraction points are better focused with 20 km aperture and amplitude dimming has been reduced in both images. Note in Figure 8.2.A, the horizontal layer at the deepest part of the section is practically continuous.

This test demonstrates that a longer migration aperture would improve the seismic image. It is important to highlight that the optimum value cannot be estimated with a 2D model. It is necessary to compute 3D full wavefield modeling not attempted in the current study.

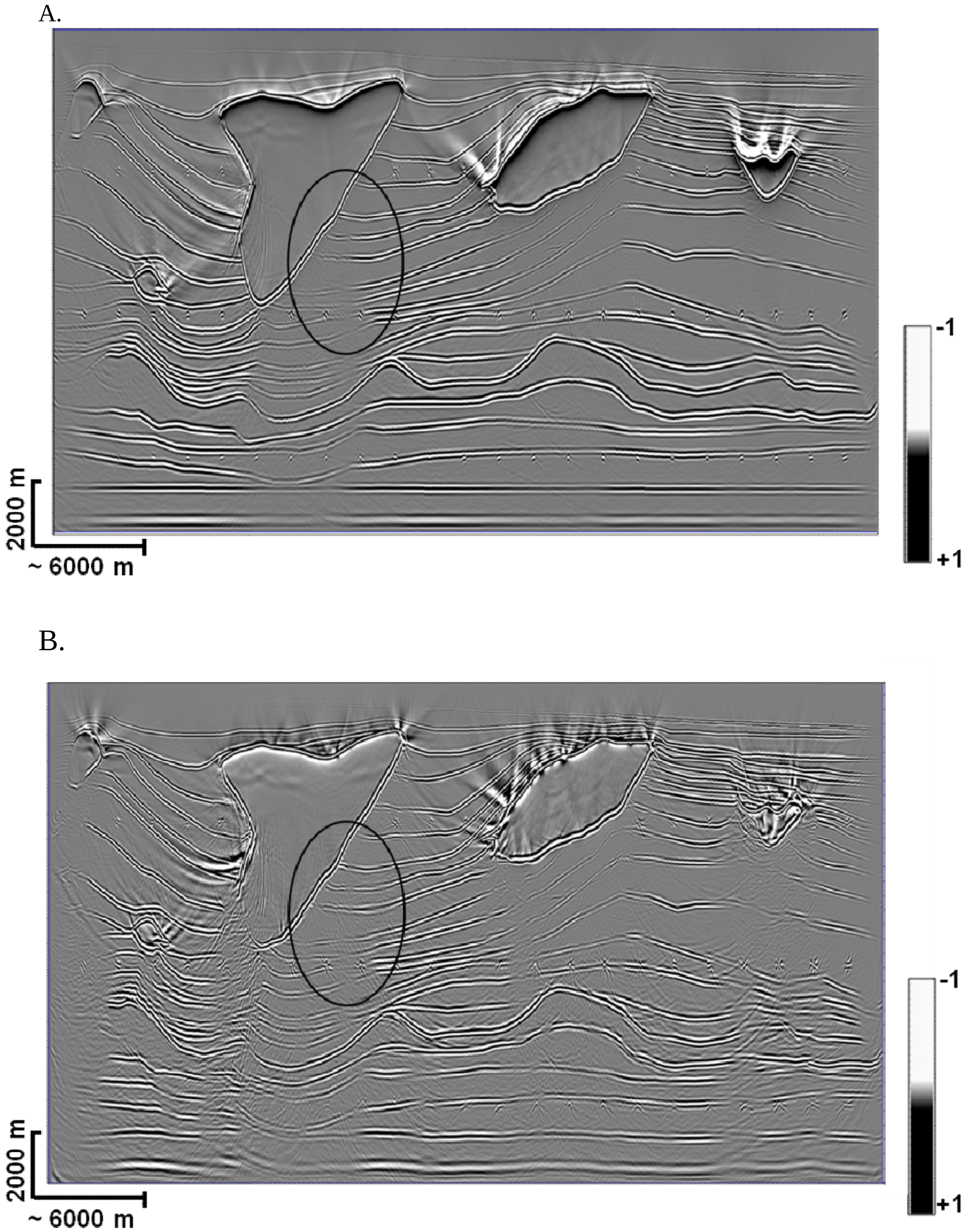

Figure 8.2. Reverse time migration results with 20 km aperture. Compare Figure 7.14. computed with 12 km aperture. A. revised velocity model. B. original velocity model. Highlight areas discussed in text.

Chapter 9

FUTURE STUDIES

This illumination study demonstrates that the available data exhibit some illumination limitations, due to orientation of salt bodies and sediments, and the distance between salt canopies. I suggest the seismic image could improve in the following ways:

Change the seismic acquisition design to full azimuth. Ray tracing results confirm that the number and distribution of azimuths should increase. The full azimuth acquisition increases fold values in every studied horizon, and also reduces shadow areas.

The offset should be larger than 8 km, according to ray tracing. On the other hand, if the offset increases then the data will contain more multiples. Another ray tracing study should be developed for the optimization of acquisition design at the target. The offset calculation should consider the energy of the rays that reach the surface and the geological model, including the short distance between the salt bodies and their orientation.

Review the velocity model. Synthetic imaging of full wavefield modeling data suggests that the base of salt should be reinterpreted. Also, the subsalt sediment velocity should change since the deepest sediments follow a linear trend, and do not consider the presence of a hard layer (Figures 7.13. and 7.14.). A better estimate of the velocity value of the hard layer would positively impact the imaging results. The interval velocity value should reflect the lithology (salt or carbonate), and consider the geological history of the region.

Also, it is important to take into account that the geological history is different on each side of the main salt body. It would be interesting to generate a local velocity model for every basin that would be tailored to local conditions.

Extend the migration aperture and consider dip inclination of the salt flanks to better capture rays coming from subsalt reflectors. Specifically, synthetic imaging of the full wavefield modeling suggests that apertures longer than 12 km could improve the accuracy of the migration results.

Another illumination study should be performed in order to quantify the optimum aperture length considering available technology. This illumination study should be in 3D and simulate full wave propagation. The full wavefield modeling computed in this study is in 2D and its virtual imaging results cannot rigourosly demonstrate the optimum aperture due to the differences between 2D and 3D modeling.

The full wavefield modeling performed in this study uses 18 km offset. It assumes the boat acquires the seismic in one direction, and then comes back recording in the opposite direction. I have shown an increase in the migration aperture from 12 km to 20 km improves the data imaging, yet the field seismic data is acquired with a streamer length equal to 8 km. A question comes to my mind: what will happen in the case that the migration aperture increases, but not the offset length? For exploration purposes, it is interesting to test this idea, since it is not always possible to acquire new data. The synthetic shot gathers can be generated again, but using 8 km offset, and later on be migrated using 20 km aperture.

The migration algorithm should include tilted transverse isotropy (TTI). Vertical transverse isotropy (VTI) could stretch the sediment layers vertically, exaggerating the subsalt steep dip planes. TTI corrects the seismic image in vertical and horizontal directions. Another illumination study should be generated including VTI and TTI, before running TTI reverse time migration. This analysis would help to understand the effect of anisotropy in the sediment layers.

3D full wavefield modeling should be computed with density variation (constant density was assumed throught this study). This would help study three dimensional effects and measure the dip-azimuth ranges that could be illuminated in the seismic image.

Include other seismic waves in the analysis. The analysis should identify the different seismic waves in both shot gathers, the real data and the full wavefield modeling, and then study the illumination limitations for each type. It is important to separate the compressional waves and the shear waves at each formation. The compressional waves can change to shear waves at the interface salt-sediments and vice versa.

Run the elastic reverse time migration. Acoustic reverse time migration is an approximation to the elastic wave equation. In theory, elastic reverse time migration can resolve the illumination limitations of the compressional wave by introducing density and shear wave velocity elastic parameters.

Chapter 10

CONCLUSIONS

I have investigated a 3D seismic dataset in the Gulf of Mexico with particular emphasis on subsalt illumination and shadow zones.

This study confirms that the studied seismic section in the Gulf of Mexico contains significant subsalt defocusing areas. Their origin can be explained by Snell's law. The maximum illumination angle that can register at surface depends on shape and orientation of the base of salt and subsalt sediments, and the salt/sediment velocity contrast. Illumination is limited when the salt flanks have a dip angle closer to the critical angle.

The extent of shadow areas can be delineated by ray tracing and depends on the seismic acquisition design.

The main characteristics of poorly illuminated areas are low fold values and amplitude dimming. For instance, in anisotropic Kirchhoff depth migration, the subsalt image is blurry, and contains multiples coming from the base of salt. Also, anisotropic reverse time migration exhibits a double image of the subsalt sediment layer terminations. Ray tracing results show the focusing areas surround the shadow regions at three different picked horizons. The focusing areas represent those subsalt regions where the rays are concentrated, recovering a higher number of rays at the surface.

Wavefronts propagate faster in the salt than in the sediments and irregularities in the base of salt or overhangs generate interference between the wavefronts at the interface salt-sediments.

The minimum distance between the shadow areas in my data is equal to 5 km. This value is measured in the deep fold map computed by ray tracing and simulating narrow azimuth acquisition. The separation between the salt bodies is small, complicating the subsalt seismic imaging. The rays are deviated by the salt body when their paths are located less than one half of the offset of the salt wedge (Muerdter and Ratcliff, 2001).

My work suggests that quality of the field seismic image could be improved by reshooting with increased offset and azimuth range.

This study also proposes to revise the velocity model, especially the base of salt and the subsalt sediment velocity trend since the original velocity model ignores subsalt high acoustic contrasts.

The aperture used in anisotropic reverse time migration of the field data was 12 km. The migration aperture should increase in order to compute a better image. The current value cannot collect all rays coming from a subsalt reflector and the steep dip base of salt reflects rays coming from the subsalt sediments. This could explain the presence of the double subsalt image, according to the synthetic imaging results of the full wavefield modeling.

Vertical transverse isotropy (VTI) should be replaced by tilted transverse isotropy in the reverse time migration algorithm. VTI assumes horizontally layered shales and stretches the seismic image vertically in order to correct the anisotropic effect. If the anisotropy is tilted then the migrated image would be stretched.

The real earth is an elastic medium, but available technology is limited and cannot simulate a 3D elastic wavefield. I believe the best algorithm that could improve seismic imaging is elastic reverse time migration that includes V_p wave velocity, V_s wave velocity, and density as inputs.

A compressional wave could be either reflected or transmitted at the salt-sediments interface as compressional wave or shear wave, or as a different kind of wave. Also, the shear wave could be converted into a compressional wave at the interface. It is recommendable to analyze the shot gathers before running elastic migration, trying to discriminate the compressional and the shear waves at every level. It is important to separate the compressional wave from the shear in order to do a quality control of the shot gathers and the seismic velocities. On the other hand, the shear wave is slower than the compressional wave, so it can exhibit different processing issues than the P-wave.

The general conclusion of this study is that the results of the integration of the ray tracing and full wavefield migration demonstrate the presence and origin of subsalt shadow zones, so the main goal has been achieved. The first part of this objective is the explanation of the origin of the defocusing areas, which has been explained by Snell's law. The second part is the delineation of the extension of the shadow areas, which has been developed by ray tracing. The third part is the improvement of seismic imaging. The quality of the image would be made better by extending azimuth and offset ranges in the acquisition design, and migration aperture. Also, the interval velocity should be revised in order to improve the quality of the seismic image.

This study demonstrates that a proper workflow can improve the seismic image. Sometimes, seismic processors only test complicated algorithms in order to improve the image. The computation costs of these algorithms are high and do not always resolve the problem. It is important to develop an illumination study to find the origin of the illumination issues and to define the proper workflow that can improve the seismic image.

Chapter 11

REFERENCES

Alkhalifah, T. and I. Tsvankin, 1995, Velocity analysis for transversely isotropic media, Geophysics, **60**, 1550 – 1566.

Audebert, F., D. Nichols, T. Redkal, B. Biondi, D. E. Lumley, and H. Urdaneta, 1997, Imaging complex geologic structure with single-arrival Kirchhoff pre-stack depth migration, Geophysics, **62**, 1533-1543.

Baud, R. D., R. H. Peterson, C. Doyle, and G. E. Richardson, 2000, Deepwater Gulf of Mexico: America's emerging frontier: Minerals Management Service Outer Continental Shelf Report 2000-022, 89 p.

Baysal, E., D. D. Kosloff, and Sherwood, J., 1983, Reverse time migration, Geophysics, **48**, 1514-1524.

Berenger, J., P., 1996, Perfectly matched layer for the FDTD solution of wave-structure interaction problems. IEEE Transactions on Antenas and Propagation, **44**, 110 – 117.

Biondi, B., 2007, Concepts and Applications in 3-D Seismic Imaging. SEG Distinguished Instructor Series, **10**, 3-40.

Bleistein, N., and S. H. Gray, 2001, From the Hagedoorn imaging technique to Kirchhoff migration and inversion, Geophysical Prospecting, **49**, no. 6, 629-643.

Billette, F., R. Clarke, J. Etgen, S.Gray, W. Rietveld, and D. Whitmore, 2000, Common-offset common-azimuth full volume 3-D pre-stack depth migration methodology. SEG Expanded Abstracts, 858-862.

Cerjan, C., D. Kosloff, R. Kosloff and M. Reshef, 1985, A non-reflecting boundary conditions for discrete acoustic and elastic wave equations, Geophysics, **50**, 705 – 708.

Cerveny, V., and I. Psencik, 1983, Gaussian beam and paraxial ray approximation in three dimensional inhomogeneous media, Bulletin of the Seismological Society of America, **70**, 47 -77.

Claerbout, J. F., 1971, Toward a unified theory of reflector mapping: Geophysics, **36**, 467-481.

Clapp, R. G. and H. Fu, 2010, Selecting the right hardware for reverse time migration, The Leading Edge, **29**, no 1, 48-58.

Clayton, R., and B. Engquist, 1980, Absorbing boundary conditions for wave equation migration. Geophysics, **45**, 895 – 904.

Docherty, P., 1991, A brief comparison of some Kirchhoff integral formulas for migration and inversion, Geophysics, **56**, 1164- 1169.

Dong, W., and G. A. McMechan, 1993, 3D pre-stack migration in anisotropic media, Geophysics, **58**, 79-90.

Du, X., R. P. Fletcher, and P. J. Fowler, 2008, A new pseudo-acoustic wave equation for VTI media: 70th Annual Conference and Exhibition, EAGE, Extended Abstracts, Paper H033.

Duveneck, E., 2008, Acoustic VTI wave equations and their application for anisotropic reverse time migration: 78th Annual Inetrnational Meeting, SEG, Expanded Abstracts, 2186-2190.

Etgen, J., 1986, Pre-stack reverse time migration of shot profiles: Standford Exploration Project, **50**, 151-170, http://sep.stantford.edu/research/reports.

Fagin, S., 1999, Model-based Depth Imaging, Course Notes Series, no. 10, Young, R.A. (Ed.), Society of Exploration Geophysicists, 27-114.

Fletcher, R.P., X. Du, P. J. Fowler, 2008, A new pseudo-acoustic wave equation for TTI media: 78th Annual International Meeting, SEG, Expanded Abstracts, 2082-2086.

Fletcher, R., X. Du, and P. J. Fowler, 2009, Reverse time migration in tilted transversely isotropic media, Geophysics, **74,** 6, 179-187

Gjøystdal, H., E. Iversen, R. Laurain, I. Lecomte, V. Vinje, and K. Åstebøl, 2002, Review of ray theory applications in modeling and imaging of seismic data, Studia Geophysica et Geodaetica, **46**, 2, 113 – 164

Hemon, C., 1978, Equations d'onde et modeles, Geophysics. Prosp., **26**, 790 – 821.

Jacobs, B., 1982, The Pre-stack migration of profiles: Ph.D. thesis, Stantford University.

Jin, S., and D. Walraven, 2003, Wave equation GSP pre-stack depth migration and illumination, The Leading Edge, **22**, 604-610.

Jones, I. F., and J. K. Fruehn, 2003, Factors affecting frequency content in preSDM imaging, The Leading Edge, **22**, 128-134.

Kelly, K. R., R. W. Ward, S. Treitel, and R. M. Alford, 1976, Synthetic seismograms: A finite-difference approach, Geophysics, **41**, 2-27.

Liao, Q., D. Ramos, W. Cai, J. Muskaj, and F. Ortigosa, 2009, Subsalt illumination analysis through ray tracing and seismic modeling: a GOM case study, 71TH EAGE Conference & Exhibition, Paper W008.

Liner, C., 2004, Elements 3D Seismology, Pennwell, 2nd edition, 3-252.

McMechan, G., 1983, Migration by extrapolation of time dependant boundary value, Geophys. Prosp., **31**, 413-430.

Meek, R. A., P. D. Anno, J. D. Brewer, and M. Coral, 2002, Anisotropic velocity model building and updating for pre-stack depth migration in Indonesia. SEG Expanded Abstracts, 145-149.

Moldoveanu, N., 2008, Circular geometry for wide-azimuth towed-streamer surveys, 70th Annual Conference and Exhibition, EAGE, Extended Abstracts, Paper G011.

Morse, P.M. and H. Feshbach, 1953, Methods in Theoretical Physics, McGraw Hill, New York, 453-600.

Muerdter, D., and D. Ratcliff, 2001, Understanding subsalt illumination through ray-trace modeling, The Leading Edge, **20**, no. 6, 578-594.

Pharez, S., N. Jones, V. Dirks, S. Zimine, H. Prigent, K. Ibbotson, and J-P. Gruffeille, 2005, Pre-stack wave-equation migration as a routine production tool, The Leading Edge **24**, no. 6, 608-613.

Ratcliff, D. W., D. J. Weber, and K. D. Sellers, 1995, Subsalt imaging via the world's largest 3D pre-stack depth migration project, Society of Exploration Geophysicists, Expanded Abstracts, 1156-1160.

Sarkar, D., and I. Tsvankin, 2003, Analysis of image gathers in factorized VTI media.

Geophysics **68**, 2016-2025.

Sava, P., and S. Fomel, 2001, 3-D travel time computation using Huygen's wavefront tracing, Geophysics, **67**, 604 – 609.

Schneider, W., 1978, Integral formulation for migration in two and three dimensions, Geophysics, **43**, 49-76.

Thomsen, L., 1986, Weak elastic anisotropy, Geophysics, **51**(10), 1954-1966.

Thomsen, L., 2002, Understanding Seismic Anisotropy in Exploration and Exploitation, the SEG/EAGE Distinguished Instructor Short Course #5 Lecture Notes, 240 pp, Soc. Expl. Geoph.

Van Trier, J., and W. W. Symes, 1991, Upwind finite-difference calculation of travel-times: Geophysics, **56**, 812-821.

Whitmore, N. D., 1983, Iterative depth migration by backward time propagation: 53rd Annual International Meeting, Society of Exploration Geophysicists, Expanded Abstracts, 382-386.

Yan, R., and X. Xie, 2009, A new angle domain imaging condition for pre-stack reverse time migration: 79th Annual International Meeting, Society of Exploration Geophysicists, Expanded Abstracts, 2784-2788.

Zhang, Y., and H. Zhang, 2009, A stable TTI reverse time migration and its implementation: 79th Annual International Meeting, Society of Exploration Geophysicists, Expanded Abstracts, 2794-2798.

Zhou, H., G. Zhang, and R. Bloor, 2006, An anisotropic acoustic wave equation for VTI media, 68th EAGE Conference and Exhibition, Extended Abstracts, Paper H033.

Appendix 1

SEISMIC ACQUISITION PARAMETERS

The seismic acquisition design was developed by GECO:

Shooting orientation: Northwest-Southeast

Recording instrument: Triacq

Streamer type: Nessie 3 & 4

Source/Receiver positioning: GPS/DGPS

Airgun source: 5400 cubic inches

Gun depth: 6 meters ± 1 meter

Sootpoint interval: 62.5 meters per CMP line

CMP crossline separation: 40 meters

Group Interval: 25 meters

Recording Channels: 320 per streamer

Streamer depth: 9 meters ± 1.5 meters

Streamer length: 8000 meters

Record length: 12.288 seconds

Sample interval: 2 miliseconds

Nominal fold: 64

Appendix 2

SEISMIC ACQUISITION

The seismic processing sequence has been divided in two main workflows:

A) Pre-stack Time Processing Sequence was performed by TGS:

- Debubble
- Noise attenuation
- Surface related multiple elimination (SRME)
- Noise attenuation
- Velocity analysis
- Radon de-multiple
- Application of cold water statics
- 3D bin sort – 12.5 m CDP interval, 58/64 fold
- Deterministic decon
- Spherical divergence and gain correction
- Grid data – 25 m x 40 m – diagonal grid
- Input migration velocities
- Kirchhoff pre-stack curved ray migration – 25 m x 40 m
- Velocity analysis
- Automatic velocity picking update at every CDP location
- Output 3D velocity trace volume (SEGY: 12.5 m by 20 m by 4 msec)
- Output ETA velocity correction trace volume (SEGY: 12.5 m by 20 m by 4 msec)

- Radon de-multiple
- Output migrated gathers with NMO/Radon
- Mute and stack

B) Wave equation migration was processed by TGS:

- Initial sediment velocity model**:** Kirchhoff 3D PSTM velocities with salt influence removed.

Wave equation PSDM model building:

- Iteration I –finite difference migration (FDMIG) for sediment model update (PSDM)
- Start point for PSDM: Output 3D volume, gathers over entire area, 50 m x 40 m grid at 20 Hz. Velocity update on 1 km x 1 km grid
- Iteration II–FDMIG for sediment model update (PSDM): Velocity update on 1 km x 1 km grid.
- Interpret salt top/model build: Top salt interpretation using FDMIG depth volume.

Salt flood for base salt:

- Iteration III- FDMIG (flood) for salt base interpretation: PSDM based salt flood model, 100 % shots input. Output 3D volume, gathers over entire area, 50 m x 40 m grid at 20 Hz

- Interpret salt base/model build: Base salt interpretation using FDMIG “flood” depth volume. Final model construction.

- Iteration IV – FDMIG output final gathers for entire image area. Output angle gathers on a 50 m x 40 m grid @ 30 Hz. Angle stack analysis and volume generation. Output raw migration.

C) Kirchhoff Depth Migration was computed by TGS:

KIRCHHOFF DEPTH MIGRATION

- Input Gathers (from time processing sequence)
- Input WEM sediment velocity field
- Half of shots and half of receivers used for velocity/model building iterations

Build Anisotropic Velocity Model

- Build 3D vertical model from well information
- Migrate the data
- Estimate anisotropic parameters delta and epsilon
- Migrate select lines to verify results – iterate above if necessary

ITERATIONS I & II - Tomography Updates

KIRCHHOFF VTI PSDM

- Input 25 m x 40 m, 29 to 32 fold, 12 seconds
- Output 50 m x 40 m, 29 to 32 fold, 16000 m depth, 10 m step

- Migration aperture 8000 m
- 2 passes of Tomography to define sediment vertical velocity field
- Update delta and epsilon if needed
- Tomography inversions at 200 m x 200 m x 50 m

ITERATION III - Define Top of Salt

KIRCHHOFF VTI PSDM

- Input 25 m x 40 m, 29 to 32 fold, 12 seconds
- Output 50 m x 40 m, 29 to 32 fold, 16000 m depth, 10 m step
- Migration aperture 10000 m with turning wave
- Interpret Top of salt.

ITERATION IV - Define Base of Salt (Salt Flood)

KIRCHHOFF VTI PSDM

- Input 25 m x 40 m, 29 to 32 fold, 12 seconds
- Output 50 m x 40 m, 29 to 32 fold, 16000 m depth, 10 m step
- Migration aperture 8000 m
- Interpret Base of salt

ITERATION V – Define Top of Salt for Overhangs

KIRCHHOFF VTI PSDM

- Input 25 m x 40 m, 29 to 32 fold, 12 seconds

- Output 50 m x 40 m, 29 to 32 fold, 16000 m depth, 10 m step
- Migration aperture 8000 m, with turning wave
- Interpret Top of salt for overhangs

ITERATION VI – Modify Base of Salt in Overhang Areas

KIRCHHOFF VTI PSDM

- Input 25 m x 40 m, 29 to 32 fold, 12 seconds
- Output 50 m x 40 m, 29 to 32 fold, 16000 m depth, 10 m step
- Migration aperture 8000 m with turning wave
- Interpret base of salt for overhangs

ITERATION VII – Subsalt Tomography Update

KIRCHHOFF VTI PSDM

- Input 25 m x 40 m, 29 to 32 fold, 12 seconds
- Output 50 m x 40 m, 29 to 32 fold, 16000 m depth, 10 m step
- Migration aperture 8000 m
- 1 pass of Tomography to define sediment velocity field below the salt
- Tomography inversions at 200 m x 200 m x 50 m

FINAL KIRCHHOFF PRE-STACK DEPTH MIGRATION WITH OVERHANGS. KIRCHHOFF VTI PSDM

- Input all shots and receivers from SRME/Radon data, 12.5 m x 40 m, 58 to 64 fold, 12 seconds
- Gathers output 50 m x 40 m, 29 to 32 fold, 16000 m depth, 10 m step (this output volume is not available).
- Migration aperture 10000 m, maximum dip 90 degrees with turning wave, frequency: 3 – 60 Hz (central frequency: 20 Hz).
- Interpolate stack volume to a 25 m by 20 m grid
- Post-stack cosmetics application

D) VTI anisotropic reverse time migration was generated by Repsol:

- Input all shots and receivers from SRME/Radon data, 12.5 m x 40 m, 58 to 64 fold, 12 seconds.
- Migration aperture 12000 m, maximum dip 90 degrees, frequency 3 – 35 Hz (central frequency: 8 Hz).
- Stack output volume, 10m step.

Appendix 3

HESSIAN MATRIX

In Mathematics, the Hessian matrix is defined as the square matrix of second-order partial derivatives of a function. The seismic Hessian matrix is computed at the same time as reverse time migration, using same input parameters, and helps to understand imaging and defocussing problems exhibit in the data. This computation represents a full illumination analysis, which depends on the velocity model.

The input parameters of the Hessian matrix are:

- Dominant frequency: 12 Hz
- Aperture: 12,000 m
- Sample increment: dx = dz = 10 m
- First sample: x = 0 m, z = 0 m
- Last sample: x = 47,880 m, z = 14,000 m

Figure 3. shows the results of the Hessian matrix using the original TGS velocity model, after high frequency filtering. The black represents the maximum illumination and white is zero.

Note that shadow areas represented in white match ray tracing results, and that subsalt sediments are affected by changes in curvature of the salt flanks. The rugosity of the salt base can cause energy focussing or shadow generation depending on details of the salt geometry. Blue circles in Figure 3. highlight shadow areas.

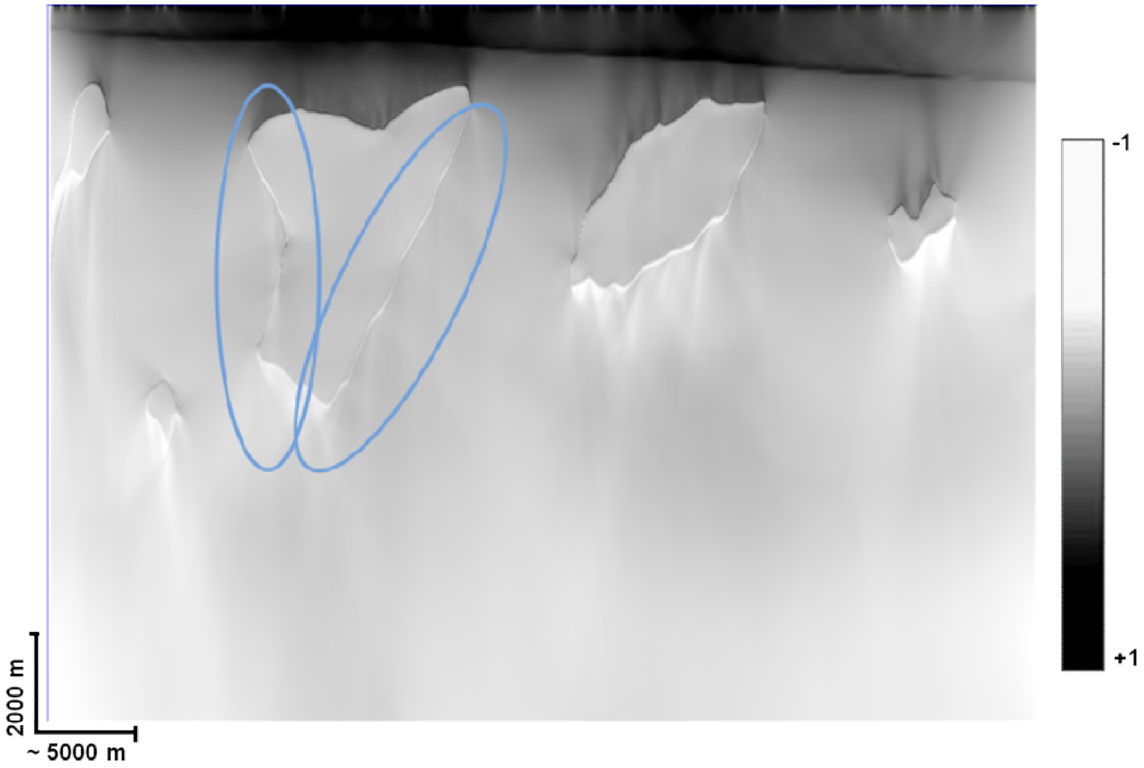

Figure 3. Hessian matrix results with original velocity model. Shadow areas are highlighted.

Figure 3. shows maximum subsalt illumination of the original velocity model for all illumination-directions.